

Libby-Sterman analysis and power-counting

Central assertions in setting up the parton model for DIS (Sec. 2.4) were that hard scattering occurs off a single parton constituent of the target, and that the hard scattering is just the Born approximation for electron-quark scattering. In fact, both assertions fail if taken literally. So in this chapter I show how to derive correct statements about the dominant configurations in DIS and the many other cases of interest. I will interleave a general treatment with a detailed discussion of specific examples.

Key insights were found by Sterman (1978) and Libby and Sterman (1978b), who systematized a correspondence between divergences in massless perturbative calculations and important configurations for high-energy processes. For any suitable process (like DIS) with an energy scale Q much larger than relevant particle masses, the main results are:

1. A one-to-one correspondence between mass divergences¹ in massless perturbation theory and non-UV regions in loop-momentum space that give the large Q asymptote.
2. That mass divergences are at surfaces where the integral over loop momenta cannot be deformed away from singularities of propagators. These surfaces are called pinch-singular surfaces (PSSs).
3. Simple and very general geometrical arguments in four-dimensional momentum space to locate the PSSs for a massless theory. The PSSs are in the typically higher-dimension space of all loop momenta.
4. Simple power-counting results for the strengths of the possible PSSs, and for the power dependence on Q of the contribution of the region associated with each PSS.
5. From the derivation of the power-counting results it is made evident what approximations are appropriate to each region, as needed to derive factorization theorems.
6. Hence error estimates are also obtained for the difference between an exact graph and its approximation in any of the regions.

These results form the logical basis of most further work in perturbative QCD, and in particular for the derivation of factorization theorems. The methods apply not only to QCD but to a general QFT.

¹ That is, divergences that appear when fields or particles are made massless, to be distinguished from ultra-violet (UV) divergences, for example.

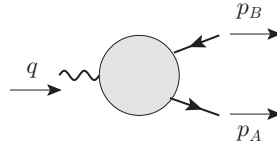


Fig. 5.1. Green function for e^+e^- annihilation to a quark-antiquark pair.

Practical calculations in QCD, as in Sec. 4.2, involve the facile manipulation of mass divergences, so that it is easy to attribute to the divergences an existence in the real world. But this is definitively incorrect: some of the fields have a non-zero mass, so that many of the mass divergences are not actually present. Moreover, even though QCD does have a massless gluon field, color confinement cuts off the divergences and prevents there from being asymptotic quark and gluon states in the exact theory.

The true relation between mass divergences and asymptotic behavior is that the PSSs for the divergences form a *skeleton* for important regions of momentum space. We use PSSs to label the regions, with the regions being *neighborhoods* of the PSSs.

As one gains experience with the methodology, the results gain a reality whose intuitive justification goes far beyond the Feynman-graph domain to which the strict mathematical justification is currently restricted. We have already explored some of these issues in Sec. 4.3, and we will see more in the generalization of the parton model to full QCD. Many of the issues have not been properly formalized. As a symptom, consider the Lund string model (Andersson, 1998), summarized in Sec. 4.3.1. This model gives a useful account of the hadronization of high-energy systems of quarks and gluons. To connect it to the fundamental underlying QCD theory, one needs to formulate the quantum-mechanical evolution of states locally in space-time in highly relativistic situations. A complete appropriate formalism is not yet available. This problem is closely related to important foundational issues in quantum mechanics and QFT.

5.1 High-energy asymptotics and mass singularities

5.1.1 Sudakov form factor, $\gamma^* \rightarrow q\bar{q}$

Many of the general principles can be discerned from a paradigmatic example, which is termed the Sudakov form factor, from its discussion by Sudakov (1956). We use the Green function for a quark field, an antiquark field, and a current (Fig. 5.1):

$$\begin{aligned} \Gamma^\mu &\stackrel{\text{def}}{=} \int d^4x d^4y e^{ip_A \cdot x + ip_B \cdot y} \langle 0 | T \psi(x) \bar{\psi}(y) j^\mu(0) | 0 \rangle \\ &= G_{\text{irred}}^\mu \times \text{full external quark propagators.} \end{aligned} \quad (5.1)$$

Here j^μ is the electromagnetic current, and ψ and $\bar{\psi}$ are fields for some flavor of quark. The photon momentum is $q = p_A + p_B$, with invariant size $Q \stackrel{\text{def}}{=} \sqrt{q^2}$. Our aim is to understand the asymptotics when Q gets large with p_A^2 and p_B^2 fixed, but not necessarily

on-shell. Factoring out external propagators gives the definition of the irreducible amplitude indicated in the last line. The off-shell amplitude appears in high-energy e^+e^- annihilation, as a subgraph of the full amplitude for the process.

In fixed-order perturbation theory, taking p_A and p_B on-shell gives IR divergences because the gluon is massless. Beyond perturbation theory, we expect color confinement in QCD to force on-shell quark amplitudes to be zero, and to cut off the IR divergences. But these issues are quite separate from the association we wish to make between properties of the large Q limit and divergences in a completely massless theory.

In setting up methods for factorization later in this book, a convenient model example is the Sudakov form factor with on-shell quarks treated in an *abelian* gauge theory, normally with a *massive gluon* (Ch. 10).

We work in the overall center-of-mass frame, oriented so that the external 4-momenta in ordinary Cartesian coordinates are

$$p_A = \frac{Q}{2} \left(1, 0, 0, \sqrt{1 - 4p_A^2/Q^2} \right), \quad (5.2a)$$

$$p_B = \frac{Q}{2} \left(1, 0, 0, -\sqrt{1 - 4p_B^2/Q^2} \right), \quad (5.2b)$$

$$q = Q(1, \mathbf{0}). \quad (5.2c)$$

5.1.2 Scaling in units of Q

Consider a particular L -loop graph G for the 1PI factor G_{irred} . Let k denote its loop momenta, and let I denote the integrand, so that

$$G = g^{2L} \int d^{nL} k I(k, p_A, p_B; m) + \text{UV counterterms}. \quad (5.3)$$

Imagine first that we were in a situation where all internal momenta have components of order Q , and have virtuality of order Q^2 . After using the renormalization group to set the renormalization scale to Q , we could use weak-coupling perturbation theory, and, to the leading power in Q , we could neglect masses. Errors in the massless approximation, from an expansion in powers of m/Q , p_A^2/Q^2 , and p_B^2/Q^2 , would be asymptotically much less than corrections from higher orders in $\alpha_s(Q)$.

Of course our initial supposition on the sizes of the internal momenta is in general false. Nevertheless, the region of k that it covers forms a useful standard for treating the general situation.

Relatively benign alternative regions are where some or all components of k are much bigger than Q . Since the external momenta are much smaller than these large components, this is the situation handled by renormalization. So let us add renormalization counterterms and then apply an RG transformation to set the renormalization scale μ of order Q . As we saw in Sec. 3.4, this procedure *effectively* cuts off the integration at around Q .

Therefore the interesting regions are where relevant components of momenta are of size Q or smaller, and where some lines have small virtuality, i.e., their momenta l obey

$|l^2| \ll Q^2$. For these lines, a lowest-order Taylor expansion in masses compared with virtuality fails. Such regions form a small part of the whole of loop-momentum space, but they can give large contributions to the integral, because of small propagator denominators.

To systematically locate relevant regions with low virtuality, we use an analysis with momenta and masses scaled in units of Q . Thus we define

$$\tilde{p}_A \stackrel{\text{def}}{=} \frac{p_A}{Q} \rightarrow \frac{1}{2} (1, 0, 0, 1), \tag{5.4a}$$

$$\tilde{p}_B \stackrel{\text{def}}{=} \frac{p_B}{Q} \rightarrow \frac{1}{2} (1, 0, 0, -1), \tag{5.4b}$$

$$\tilde{q} \stackrel{\text{def}}{=} \frac{q}{Q} = (1, \mathbf{0}), \tag{5.4c}$$

where the limits apply as $Q \rightarrow \infty$. The scaled external quark and antiquark momenta become light-like, while \tilde{q} is a fixed time-like vector. Similarly we have scaled loop momenta, $\tilde{k} \stackrel{\text{def}}{=} k/Q$, and mass(es), $\tilde{m} \stackrel{\text{def}}{=} m/Q \rightarrow 0$.

Dimensional analysis applied to (5.3) gives

$$G = Q^{D(G)} g^{2L} \int d^{nL} \tilde{k} I(\tilde{k}, \tilde{p}_A, \tilde{p}_B; \tilde{m}) + \text{UV counterterms.} \tag{5.5}$$

Here $D(G)$ is the dimension of the integral (in powers of energy), with the coupling excluded. In a space-time dimension $n = 4 - 2\epsilon$, we have

$$D(G) = nL + \dim I = \dim G - 2L \dim g = -2L\epsilon. \tag{5.6}$$

Equations (5.4) and (5.5) show that the infinite Q limit at fixed mass is closely linked to the zero-mass limit at fixed Q , in the scaled integral on the right-hand side of (5.5). As observed earlier, if there were no singularities in the zero-mass limit, we could just set $p_A^2 = p_B^2 = m^2 = 0$ to obtain an elementary RG-controlled calculation of the large Q behavior. Moreover, the Q dependence would just be $Q^{D(G)}$. From (5.6), we see that because of the dimensionless of a gauge theory coupling at the physical space-time dimension, the power of Q is the *same* for all graphs, viz. zero.

5.1.3 Importance of pinch-singular surfaces in massless limit

We now need to locate the situations where the zero-mass limit fails. These situations arise from regions where one or more lines have virtuality much less than Q^2 . But often the contour of integration can be deformed away from such regions, and the above scaling arguments work equally well on a deformed contour for k . So our concern is regions where there is an obstacle to any possible deformation to where the lines have virtuality of order Q^2 . In fact, as we now show, the only obstacles are those that give a pinch-singular surface (PSS) in the massless limit.

Consider first some region of scaled loop momentum \tilde{k} where certain propagator denominators are not part of a pinch in the massless theory. Then in the scaled integral and on some deformed contour, these denominators have a non-zero minimum size. In the original

integral, before scaling, the same denominators have a minimum size proportional to Q^2 in the corresponding region of k . Then the simple massless limit applies for the contribution to the large Q asymptote by these denominators.

Next we consider unscaled momenta in a neighborhood of a PSS of the massless theory. Even with a massless PSS, the minimum virtuality of *unscaled* lines often stays finite as Q gets large, even on a deformed contour. Typically, this virtuality would be of order a mass-squared. But in some cases the minimum virtuality may grow with Q , but less rapidly than Q^2 , for example, it might be of order Qm . Even so, in all these cases, the scaled virtuality, i.e., relative to Q^2 , goes to zero as $Q \rightarrow \infty$. This corresponds to an exact pinch in the massless theory: that is, with masses set to zero, the scaled momenta \tilde{k} in (5.5) have a minimum distance of zero from the lines participating in the PSS.

In the actual case, with non-zero masses and finite Q , the relevant momenta are forced to go close to the PSS, the closeness in units of Q decreasing as Q increases. I summarize this by saying that the PSSs of the massless theory form a skeleton for the important non-UV regions of loop momentum space. This can happen even in a field theory where all the fields have non-zero mass, so that the exact massive theory has no literal PSS.

5.1.4 Location of pinch-singular surfaces: Landau criterion

Therefore we now have to find all possible PSSs in the massless limit and determine their strengths. The general task of locating PSSs is made quite simple by the Landau criteria (e.g., Eden *et al.*, 1966) in the form particularly emphasized by Coleman and Norton (1965): The PSSs (for the physical region, which is all that concerns us) are where the on-shell propagators and momenta correspond to classically allowed scattering processes treated in coordinate space.

Each point on a PSS (in loop momentum space) corresponds to a space-time diagram obtained as follows. First we write a reduced graph by contracting to points all of the lines whose denominators are not pinched. Then we assign space-time points to each vertex of the reduced graph so that the pinched lines and their momenta correspond to classical particles. That is, to each line we assign a particle propagating between the space-time points corresponding to the vertices at its ends. The momentum of the particle is exactly the on-shell momentum carried by the line, correctly oriented to have positive energy. If, for some set of momenta, it is not possible to construct such a reduced graph, then we are free to deform the contour of integration.

Although our argument to this point was presented in the context of the Sudakov form factor, it is in fact a general argument and can be applied to many processes with a large scale Q .

5.2 Reduced graphs and space-time propagation

The construction of the most general reduced graph becomes extremely simple in the zero-mass limit, since at a PSS all pinched lines must carry either a light-like momentum or zero

momentum. Moreover, each light-like momentum must be parallel to one of the light-like external lines.

To understand this, we just need to obtain the simple rules for how massless on-shell momenta combine at vertices of a reduced graph.

1. First, adding zero momentum to anything leaves the second momentum unaltered. So a zero-momentum line can attach anywhere.
2. Two non-zero light-like momenta in the same direction are proportional to each other and add to make another parallel light-like momentum, with a special case of giving zero when they are equal and opposite. If we orient the momenta of the lines for a particular light-like direction so that they all have positive energy, then as we follow them forward, the momenta can split and recombine arbitrarily, but the total momentum is fixed.
3. Adding two non-zero light-like momenta with *different* directions produces a non-light-like momentum, necessarily off-shell in a massless theory. Either the non-light-like momentum is external or it is on an internal line. An external non-light-like momentum would be like the virtual photon in the form factor or in DIS. An internal line is off-shell, so it is internal to a reduced vertex, i.e., it does not participate in the pinch under discussion.
4. It is possible for a reduced vertex to correspond to a non-trivial wide-angle scattering of massless particles. But for the classical scattering condition to hold, the other ends of the light-like lines are a long way from the reduced vertex. So further rescattering of the same particles is not possible. See the discussion of Fig. 5.3 below on p. 94 for an example.

The results for massless PSSs can be presented in two forms: (a) the structure of the reduced graphs, with a labeling of lines by momentum type, and (b) the locations of the vertices of the corresponding classical processes in space-time; see the illustrative examples in Sec. 5.3 below.

It is convenient to present the results with the aid of massless but unscaled momenta corresponding to high-energy external lines. For example, in the case of Fig. 5.1, from the limits in (5.4a), we define unscaled massless momenta by

$$p_{A,\infty} \stackrel{\text{def}}{=} \frac{Q}{2} (1, 0, 0, 1), \quad (5.7a)$$

$$p_{B,\infty} \stackrel{\text{def}}{=} \frac{Q}{2} (1, 0, 0, -1). \quad (5.7b)$$

5.3 Examples of general reduced graphs

5.3.1 Vertex graph

For the vertex graph of Fig. 5.1, a typical reduced graph and the corresponding space-time diagram are shown in Fig. 5.2. In the reduced graph, there is a subgraph H which includes

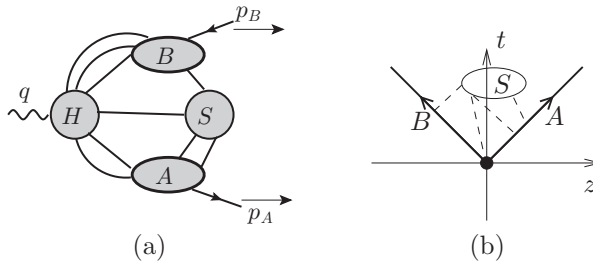


Fig. 5.2. Typical (a) reduced graph, and (b) space-time diagram, for a general PSS for the vertex graph.

the vertex for the current j^μ . This subgraph is intended to be a vertex of the reduced graph, i.e., none of its lines participate in the pinch. Thus, in the space-time diagram all of the lines and Feynman-graph vertices that compose H are contracted to a single point.

From H exit two sets of lines in what we call collinear subgraphs. One collinear subgraph, A , has lines in the $p_{A,\infty}$ direction, and the other, subgraph B , has lines in the $p_{B,\infty}$ direction. Finally the soft subgraph S , not necessarily connected, consists of lines of zero momentum at the PSS, and it can connect to any of the other subgraphs. Notice that we labeled the collinear graphs by the light-like momenta $p_{A,\infty}$ and $p_{B,\infty}$ rather than the actual external momenta p_A and p_B , since we are discussing PSSs in the massless limit.

In the space-time picture the hard subgraph corresponds to a single point at the origin, and the collinear subgraphs A and B correspond to propagation outward along light-like directions. Within each collinear subgraph, there can be arbitrary splitting and recombination of the collinear momenta. Any number of lines can join the A and B subgraphs to the H subgraph. Finally the S subgraph corresponds to zero momentum and so to arbitrarily large separations in space and time. The zero-momentum lines can interact arbitrarily with each other, and any number of lines can connect their subgraph to the other subgraphs.

From the reduced diagram point of view, the collinear and soft subgraphs contain lines of the stated kind, i.e., parallel to $p_{A,\infty}$, $p_{B,\infty}$, or zero. But it should be noted that the reduced-graph vertices that join them within each subgraph may comprise non-trivial (one-particle-irreducible) graphs from the Feynman graph point-of-view.

The collinear lines go outward from the hard vertex and eventually combine to form the momenta $p_{A,\infty}$ and $p_{B,\infty}$ of the outgoing external lines of the vertex, treated as massless momenta. There can be no other massless lines propagating in other directions, or from the past. Any such line would just give a dangling end with no external line(s) to absorb or generate the non-zero momentum.

These conclusions depend not only on the on-shell condition for the lines of the reduced graph, but, critically, also on the condition that they correspond to a physical scattering. As an example, consider the configuration illustrated in Fig. 5.3. Here there are two intermediate massless on-shell lines with 3-momenta not along the z axis:

$$p_{C,\infty} = \frac{Q}{2}(1, \mathbf{n}), \quad p_{D,\infty} = \frac{Q}{2}(1, -\mathbf{n}). \tag{5.8}$$

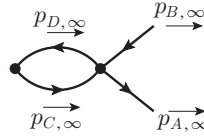


Fig. 5.3. Non-pinched on-shell configuration for Sudakov form factor.

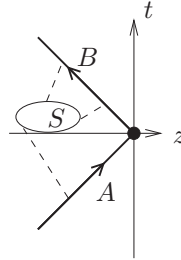


Fig. 5.4. Space-time diagram for PSSs for the vertex graph when the A line is incoming, so that the momentum transfer is space-like.

These rescatter at the right-hand reduced vertex to make the standard external lines. This reduced vertex is for elastic scattering with large momentum transfer. The on-shell configuration obeys momentum conservation, and does contribute in a computation of the imaginary part of the amplitude from on-shell intermediate states. But for the rescattering to be classical, in the sense used for the Landau criterion, the two wide-angle particles have to meet at a single point to rescatter. Thus they would travel only a zero distance from their generation at the electromagnetic vertex, and not the arbitrary non-zero distance needed for classicality. Hence this configuration does not participate in a pinch.

A minor variation can be made by letting the p_A line be incoming rather than outgoing, with the momentum transfer now being space-like. This would be appropriate for a subgraph inside a deeply inelastic scattering amplitude. The general reduced graphs stay the same, except for the orientation of the momenta in the A subgraph. Correspondingly, the space-time structure changes to that shown in Fig. 5.4.

5.3.2 Leading regions for vertex graph

Comparing Fig. 5.2(a) to the structure Fig. 2.5(b) that was used to obtain the parton-model formula for DIS, we see a lot of extra connections between the subgraphs. This endangers the derivation of a factorization theorem. In the parton-model ansatz for DIS, the hard scattering involves only a *single* parton, and the target and outgoing collinear subgraphs are not otherwise coupled. Similar remarks evidently apply to all other processes.

When we derive rules for power-counting, later in this chapter, we will find that for many of the massless PSSs, the corresponding contributions to the actual vertex are in fact suppressed by a power of Q . Generally, we will neglect these power-suppressed

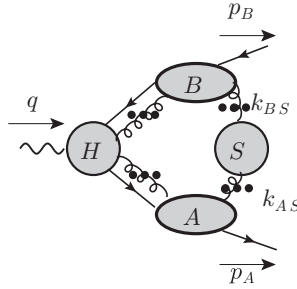


Fig. 5.5. Typical reduced graphs for the vertex graph, but now restricted to those PSSs relevant for the leading power.

contributions. Then we will find that the leading regions for the Sudakov form factor are restricted to those of Fig. 5.5. Compared with the general PSS, Fig. 5.2(a), the changes are that: no lines connect S to H , only gluons connect S to the collinear subgraphs, and exactly one fermion but arbitrarily many gluons connect the collinear subgraphs A and B to the hard subgraph.

The arbitrary number of gluons linking the different subgraphs of a reduced graph still leaves us with an apparent difficulty for proving factorization. A final power-counting result will come to the rescue, concerning the dominant polarization for the extra gluon connections.

Here we only summarize what we will prove later. The relevant polarizations are such as to allow us to use Ward identities to sum over the ways of connecting the extra collinear gluons to the hard subgraph and of connecting the soft gluons to the collinear subgraphs. The end product will be a factorized form, with definitions of parton densities and other non-perturbative quantities as matrix elements of certain non-local operators. Without the extra gluon connections, the operators would not be gauge invariant. Summing the extra gluon connections between the subgraphs converts the operators to a gauge-invariant form.

5.3.3 DIS from uncut amplitude

A very straightforward application of the Landau analysis is to DIS, if we apply the same trick as we used in Sec. 4.4 for the $e^+e^- \rightarrow$ hadrons cross section.

Instead of the hadronic tensor $W^{\mu\nu}$ defined by (2.18), we use the corresponding uncut amplitude² where the current operators are time-ordered:

$$T^{\mu\nu}(q, P) = \frac{1}{4\pi} \int d^4z \, e^{iq \cdot z} \langle P, S | T J^\mu(z/2) J^\nu(-z/2) | P, S \rangle. \quad (5.9)$$

This amplitude is analytic in the plane of $\nu = p \cdot q$, with cuts along the positive and negative real axis starting from $\nu = \pm Q^2/2$ (Fig. 5.6). The ordinary hadronic tensor is the

² Warning: Definitions in the literature disagree on the normalization.

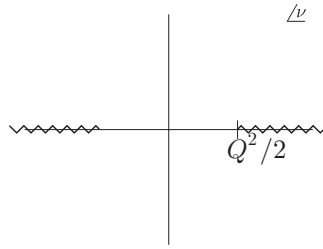


Fig. 5.6. Complex plane in $\nu = P \cdot q$ for $T^{\mu\nu}$, with its cuts.

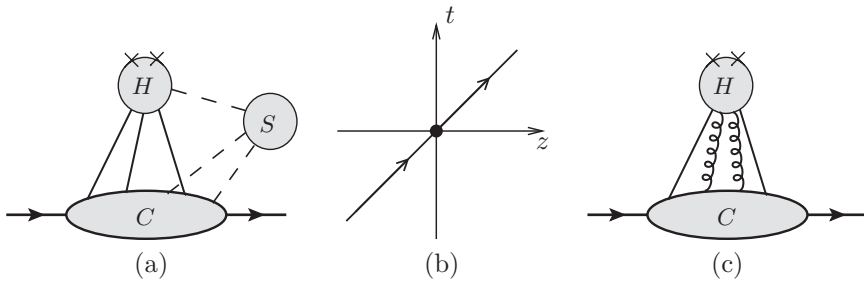


Fig. 5.7. (a) Typical general reduced graph, and (b) space-time diagram, for the most general PSS for the uncut amplitude for DIS. (c) For a leading PSS, there is no soft part, and beyond the main partons, an arbitrary number of gluons connect the collinear and hard subgraphs.

discontinuity

$$W^{\mu\nu}(q, P) = T^{\mu\nu}(\nu + i0) - T^{\mu\nu}(\nu - i0). \tag{5.10}$$

See Ch. 14 of Collins (1984) for more details and an account of earlier work on DIS. There the analyticity properties of $T^{\mu\nu}$ were exploited to allow the use of the short-distance operator product expansion to analyze integer moments of DIS structure functions.

Just in e^+e^- annihilation (Sec. 4.4), a local averaging should be applied, after which we only need to treat $T^{\mu\nu}$ away from its singularities in the complex plane.

The massless PSSs for the amplitude are illustrated by the reduced graph in Fig. 5.7(a). There is a single collinear subgraph C , where the target comes in and undergoes arbitrary collinear splittings and recombinations until the target is reconstituted. The hard scattering H is at the origin in space-time, and there is a soft subgraph S . In a general PSS, there are arbitrarily many lines joining the subgraphs. The graphical structure, Fig. 2.5(b), that we used to formulate the parton model is the simplest example. It corresponds to a minimal PSS where only two lines join the collinear and hard subgraphs, where there is no soft subgraph, and where the hard subgraph is a lowest-order Feynman graph.

The Landau analysis has now indicated, in Fig. 5.7(a), the maximum complication to be considered in the general case. We can again anticipate the power-counting results, in Fig. 5.7(c). At leading power, the soft subgraph is absent. The connections between the collinear and hard subgraphs consist of the primary pair of parton lines, just as in the

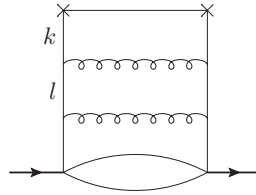


Fig. 5.8. A graph for uncut amplitude for DIS with multiple PSS.

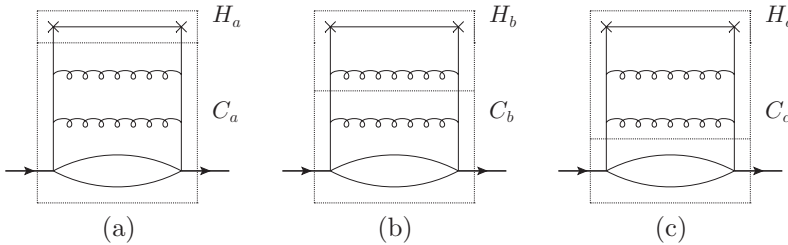


Fig. 5.9. The three leading regions for Fig. 5.8 correspond to these decompositions into hard and collinear subgraphs.

parton model, but they are now accompanied by any number of gluon lines with the special polarization that allows the use of Ward identities to give a factorization theorem.

5.3.4 Higher-order corrections to hard scattering

The following consequence of the general region analysis contains a critical difference between the true results of QCD and the parton model: This is that there are higher-order perturbative corrections to the hard scattering.

Although we will work out the details only in later chapters, it is possible to understand the basic ideas from our analysis so far. First we observe that any particular Feynman graph might have multiple leading PSSs. For example, consider Fig. 5.8, which can appear in a model for DIS in which the target is treated as elementary. This graph, of the form of what is often called a “ladder graph”, has three decompositions of the form of Fig. 5.7(c), but, in this particular case, without any of the extra gluonic connections. In one of its PSSs all the quark lines on the sides of the ladder are collinear to the target, i.e., the momenta k and l are target-collinear. This corresponds to the decomposition of Fig. 5.9(a), where the hard subgraph H_a is the smallest possible, and is indeed exactly the same as in the parton model.

A second PSS corresponds to Fig. 5.9(b), where the upper loop momentum k is of high virtuality, while the lower momentum l is still target-collinear. This has a one-loop hard subgraph H_b . Physically it corresponds to production of two jets in the hard scattering, as in the experimental event shown in Fig. 5.10. A third PSS corresponds to Fig. 5.9(c), where both k and l are of high virtuality; this situation corresponds to production of three jets.

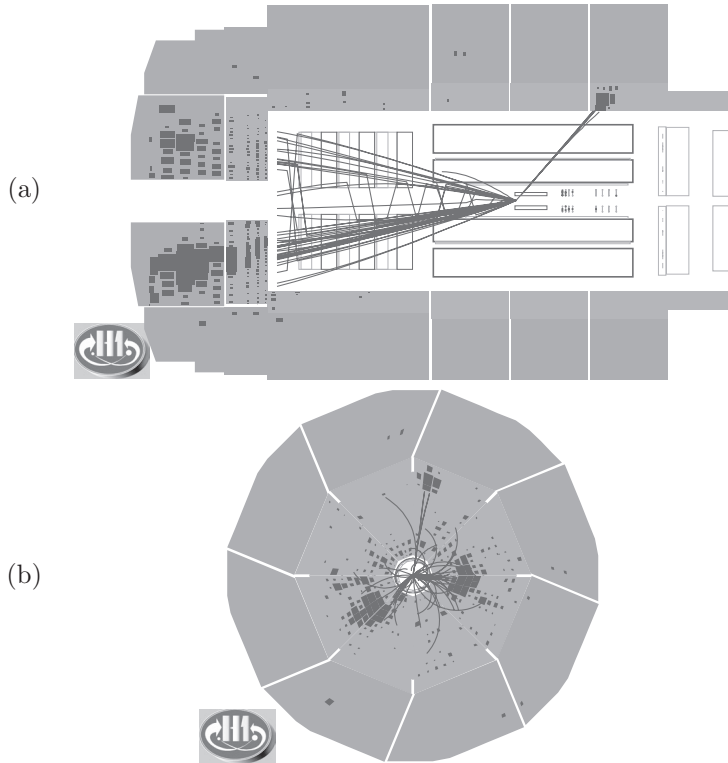


Fig. 5.10. Scattering event with two high-transverse-momentum jets in an ep collision in the H1 detector (H1 website, 2010). The final state contains an electron track (to the right in the side view), and two jets of hadrons.

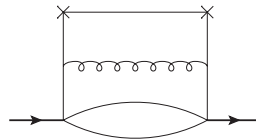


Fig. 5.11. Another graph for uncut amplitude for DIS in which some of the same hard subgraphs occur as for the previous graph.

Each of these hard-scattering subgraphs can occur in other graphs for $T^{\mu\nu}$. For example, the hard subgraphs H_a and H_b also appear in PSSs for Fig. 5.11.

The momentum regions associated with the three PSSs are represented in Fig. 5.12, where the smaller PSSs are boundaries of the bigger ones. Disentangling the contributions associated with different PSSs gives interesting mathematical and technical issues, which occupy much of this book.

We will see that larger hard subgraphs H_b , etc., can be treated as higher-order corrections to the lowest-order subgraph H_a , but with subtractions to compensate for double counting between different contributions.

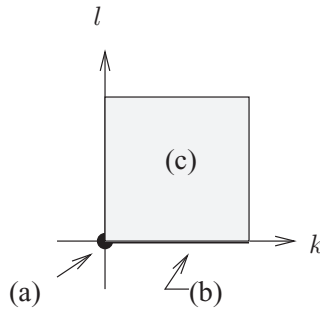


Fig. 5.12. Momentum regions associated with the PSSs in Fig. 5.9. Each axis corresponds to the deviation of the associated momentum from exact collinearity, and the labels “(a)”, “(b)” and “(c)” correspond to the PSSs associated with the graphical decompositions in Fig. 5.9.

The idea of higher-order corrections to the hard scattering is readily accommodated by the original space-time motivation for the parton model. This asserted that the cross section was governed by a short-distance scattering of the electron and a single constituent of the target, as in Fig. 2.2. The true hard scattering is the short-distance structure at the origin in the space-time representation, Fig. 5.7(b), but it need not be a lowest-order graph.

A scaling argument of the kind given in (5.5) shows that the power of Q is determined only by the number of external lines of the hard scattering, in any renormalizable theory like QCD, since then the coupling is dimensionless. Thus there is no power-law suppression of higher-order hard scattering. The only suppression is from the smallness of the effective coupling $\alpha_s(Q)$ at large Q . The appropriate scale for the coupling in the hard scattering is of order Q , so that the asymptotic freedom of QCD allows low-order perturbation theory to give useful predictions of the hard scattering.

Physically, the hard subgraph H is not literally at a single point, but is spread over a space-time range of order $1/Q$. Similarly, the collinear subgraph is not exactly on the light-like line indicated in Fig. 5.7(b), but is spread out as appropriate for a highly boosted composite particle. Lorentz contraction indicates that the width of the collinear lines is of order $1/Q$ in the t - z plane, but of order $1/M$ transversely, while time dilation gives a large longitudinal scale to Fig. 5.7(b), of order Q/M^2 . This interpretation is another way of explaining the statement that the massless PSSs form a skeleton for the location of the actual physical phenomena. A formal derivation from first principles within QFT of the detailed space-time interpretation would be very useful.

5.3.5 DIS from cut amplitude

To understand how the final states in DIS arise, we now restore the final-state cut. It is evident from our calculations of e^+e^- annihilation that there is a close connection between divergences from virtual gluon emission and those from real gluon emission. Therefore, it is useful to extend our analysis with reduced graphs and space-time diagrams to include the integrals over final states.

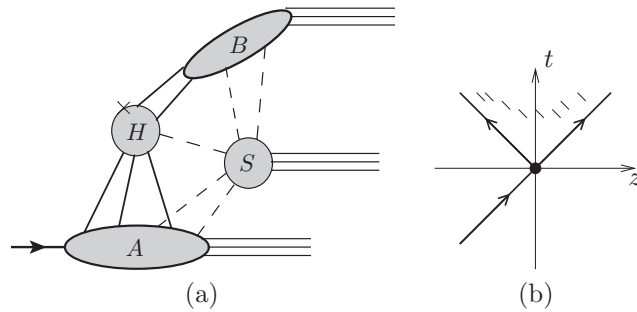


Fig. 5.13. (a) Reduced graphs and (b) space-time diagram, for DIS amplitude, in the case that only one jet arises from the hard scattering. The lighter hatching at the top of (b) corresponds to the low momentum or soft particles from the soft subgraph S .

The basic idea is unchanged: taking $Q \rightarrow \infty$ at fixed mass is equivalent to a massless limit at fixed Q , and we need to know where propagator denominators fail to have virtuality of order Q^2 . Just as before, it is the locations of PSSs in the massless theory that label all the interesting regions. But for final-state lines, we no longer have to appeal to a technical argument as to whether or not a contour deformation is possible. Final-state lines are necessarily on-shell, so they have to be considered always pinched. Since final-state particles can be observed, it is appropriate not to even consider deforming any of the integrals over final-state momenta. Some lines are not part of any loop, as in the real emission graphs considered in Ch. 4; their virtuality is entirely determined by the external lines. At a collinear singularity, it is simply from the topology of the graph plus the simple rules for combining light-like momenta that we get the condition of a classical process. We supplement this by the Landau criterion for lines that are part of a loop.

In the case that we only have one direction for the particles from the hard scattering, the reduced diagrams and space-time picture are shown in Fig. 5.13, for an amplitude $\langle X, \text{out} | j | 0 \rangle$. These correspond quite directly to the picture shown in Fig. 2.2, and the actual scattering event in Fig. 2.3. The collinear subgraph A corresponds to the target hadron, its evolution and its remnants after a quark has been struck out of it. The remnants are around the beam pipe in the actual event. The subgraph B corresponds to collinear evolution of the struck partonic system into an observed jet. Some lines can go out to the final state from the S subgraph; at the exact mass singularity, these have zero momentum. The corresponding actual particles, all of whose momentum components are much less than Q to be close to the PSS, are those that fill in the rapidity gap between the jet and the beam remnant.

Other PSSs arise when there are two or more groups of parallel lines emerging from the hard scattering, as in Fig. 5.14. In experiments one manifestation of momentum configurations near to such singularities are events with extra jets, as in Fig. 5.10.

Naturally, the full DIS cross section has an integral over all accessible final states. This integral includes all intermediate configurations between the extremes given by the reduced diagrams and their associated massless PSSs. Proper factorization theorems, and their proofs, handle the intermediate cases once the extremes are dealt with.

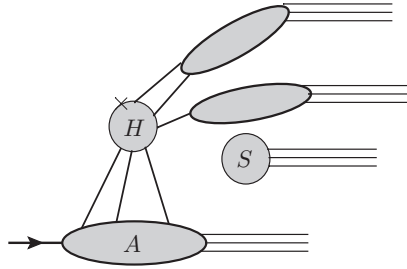


Fig. 5.14. Reduced graph for DIS, in the case that partons in more than one direction arise from the hard scattering. For clarity the connections between the soft subgraph and the other subgraphs have been omitted.

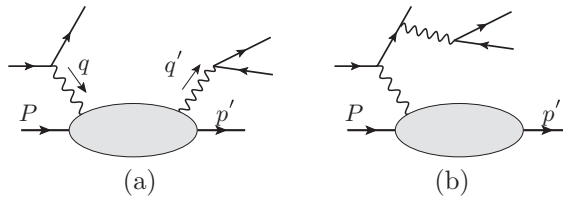


Fig. 5.15. (a) The double deeply virtual Compton scattering process, including the attached leptons. (b) The Bethe-Heitler pair production process that also contributes to the scattering.

5.3.6 Deeply virtual Compton scattering, etc.

So far, we have treated the uncut hadronic tensor $T^{\mu\nu}$ merely as a tool for analyzing DIS, whose true cross section arises from the discontinuity, i.e., from the cut amplitude.

But it is also interesting to examine this quantity in its own right as the hadronic part of an appropriate scattering amplitude. It actually provides the conceptually simplest of all QCD factorization theorems. We therefore take the opportunity to introduce the relevant processes. For this, we attach leptons at the other ends of virtual photon lines. To obtain a realizable scattering, one of the virtual photons is time-like, creating a lepton pair. Thus the relevant process is $lP \rightarrow l'p'e^+e^-$ or $lP \rightarrow l'p'\mu^+\mu^-$; Fig. 5.15(a). Since one photon has space-like momentum q and the other has time-like momentum q' , the hadronic amplitude is not diagonal, unlike the case for DIS. A complication for the analysis of data is that one needs to separate the contribution where the lepton pair arises from a virtual photon attaching to the other leptons: Fig. 5.15(b).

This leads (Müller *et al.*, 1994; Blümlein and Robaschik, 2000) to the study of the process $\gamma^*(q) + P \rightarrow \gamma^*(q') + p'$, which corresponds to the off-diagonal hadronic tensor

$$\begin{aligned}
 &A^{\mu\nu}(\gamma^*(q) + p \rightarrow \gamma^*(q') + p') \\
 &= \frac{1}{4\pi} \int d^4z e^{iz \cdot (q+q')/2} \langle p' | T J^\mu(z/2) J^\nu(-z/2) | P \rangle. \tag{5.11}
 \end{aligned}$$

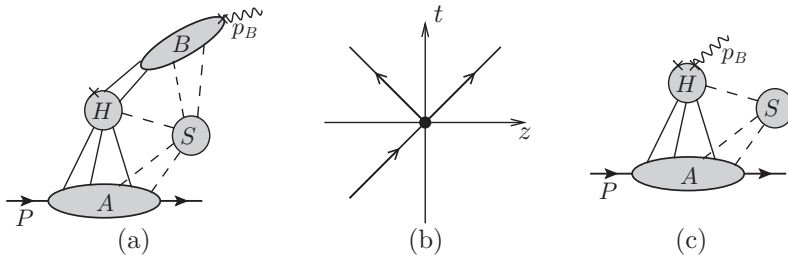


Fig. 5.16. (a) Reduced graphs and (b) space-time diagram, for DVCS and exclusive electroproduction of mesons. (c) Extra reduced graphs for DVCS, but *not* exclusive meson electroproduction, with photon directly connected to H .

This was investigated by Berger, Diehl, and Pire (2002), who called it “timelike Compton scattering”, and then by Guidal and Vanderhaeghen (2003), who called it “double deeply virtual Compton scattering” (DDVCS), the term we use here. The analysis closely corresponds to the DIS case, when we take a generalized Bjorken limit. In this limit q^2 , q'^2 , etc. are large, and the hadron momenta P and p' become parallel.

Thus the analysis in terms of massless PSSs is identical to that for $T^{\mu\nu}$ for DIS; the reduced graphs and space-time picture are exactly the same. DDVCS has great fundamental importance as the simplest quantity to which factorization methods can be applied. However the cross sections at the leptonic level are high order in electromagnetism and thus very small; see Berger, Diehl, and Pire (2002); Guidal and Vanderhaeghen (2003).

What is studied experimentally at present is the case that the outgoing photon is real. This is deeply virtual Compton scattering (DVCS): Müller *et al.* (1994); Blümlein and Robaschik (2000); Belitsky, Müller, and Kirchner (2002):

$$\gamma^*(q) + P \rightarrow \gamma(p_B) + p'. \quad (5.12)$$

The outgoing photon is light-like in what we can choose to be approximately the $-z$ direction. Thus it is convenient to change notation to use p_B for the photon momentum; this corresponds to our notation for other processes with two high-energy particles. Another closely related process has the photon replaced by a meson:

$$\gamma^*(q) + P \rightarrow M(p_B) + p', \quad (5.13)$$

the measured meson being typically a ρ . This is actually an exclusive two-body subprocess of DIS, called exclusive electroproduction of mesons. The reduced graphs now acquire a collinear- B subgraph going out from the hard scattering, Fig. 5.16(a), with a corresponding space-time diagram. The power-counting is a bit more subtle, and depends on the polarization of the meson (Brodsky *et al.*, 1994; Collins, Frankfurt, and Strikman, 1997).

For the case of a photon, i.e., DVCS, there are also reduced graphs without the B subgraph, i.e., with the photon connecting directly to the hard subgraph. These are, of course, the same as for a highly virtual photon; it is these reduced graphs that turn out to be the leading ones (Müller *et al.*, 1994; Blümlein and Robaschik, 2000; Belitsky, Müller, and Kirchner, 2002).

5.3.7 Drell-Yan process

Another important process is the Drell-Yan (DY) process, i.e., inclusive production of high-mass lepton pairs in hadron-hadron collisions:

$$P_A + P_B \rightarrow (\gamma^* \rightarrow l^+l^-) + X, \tag{5.14}$$

where we have indicated that in lowest order in electromagnetism, the lepton pair arises from a virtual photon. Essentially all the same theoretical considerations apply to the production of high-mass electroweak bosons, like the W , Z , and Higgs particle, as well as innumerable conjectured particles in extensions of the Standard Model.

In light-front coordinates, we write the momenta as

$$P_A = (P_A^+, m_A^2/2P_A^+, \mathbf{0}_T), \tag{5.15a}$$

$$P_B = (m_B^2/2P_B^-, P_B^-, \mathbf{0}_T), \tag{5.15b}$$

$$q = \left(x_A P_A^+ \sqrt{1 + q_T^2/Q^2}, x_B P_B^- \sqrt{1 + q_T^2/Q^2}, \mathbf{q}_T \right). \tag{5.15c}$$

Here the scaling variables are defined by

$$x_A = Qe^y/\sqrt{s}, \quad x_B = Qe^{-y}/\sqrt{s}, \tag{5.16}$$

where $y = \frac{1}{2} \ln \frac{q^+ P_B^-}{q^- P_A^+}$ is the center-of-mass rapidity of the lepton pair, and $Q = \sqrt{q^2}$ is its invariant mass. In the center-of-mass, the large components of the hadron momenta are P_A^+ and P_B^- , both equal to $\sqrt{s}/2$ up to power-suppressed corrections. Frequently, the cross section is integrated over q_T , and is presented as $d^2\sigma/(dQ^2 dy)$.

We first discuss the DY amplitude. Its reduced graphs are constructed by an elementary generalization of the construction for DIS. We now have two collinear subgraphs, A and B , associated with each incoming particle. As in DIS, we classify the reduced graphs by the number of outgoing directions of lines from the hard scattering H . Now H has incoming lines from each of the A and B subgraphs, and has the virtual photon taking out momentum. This allows the minimal situation, illustrated in Fig. 5.17, with no extra collinear groups at all going out from H . The soft subgraph can create particles in the final state that fill in the rapidity gap between the beam remnants.

This is illustrated by the microscopic view of a collision shown in Fig. 5.18 (which corresponds to Fig. 2.2 for DIS). Here we have shown the simplest possibility: a single parton from each parent hadron collides over a short distance scale, of order $1/Q$ at the position indicated by a star, and we have not depicted the possible soft interactions.

One new possibility is that we could have a second hard part, disconnected from the first in which other collinear lines from A and B collide to undergo a wide-angle scattering. Physically, this corresponds to a second partonic collision in Fig. 5.18, typically occurring at about the same time as the one that creates the DY pair, but at a different transverse separation. Later, from the power-counting rules, we will see that this case is power-suppressed.

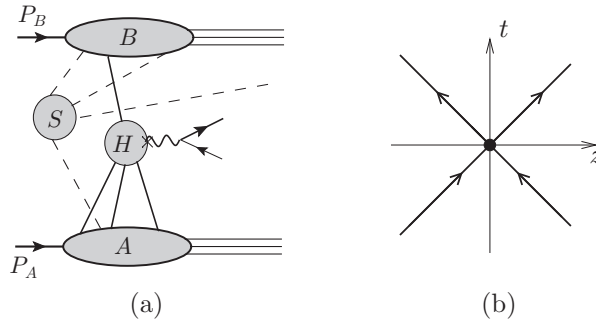


Fig. 5.17. (a) An important reduced graph for the amplitude for the Drell-Yan process. (b) Space-time diagram for collinear subgraphs.



Fig. 5.18. Microscopic view of a DY process, corresponding to Fig. 2.2 for DIS.

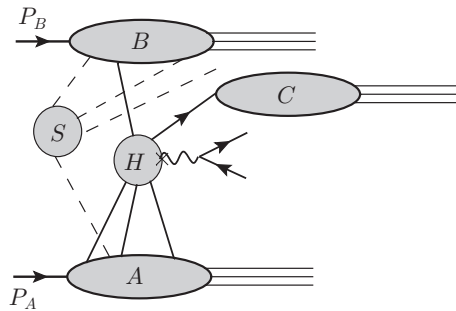


Fig. 5.19. A reduced graph for the amplitude for Drell-Yan process when one extra jet of high transverse momentum is produced.

After this, we will find the usual situation for the leading power that only one main parton from each beam hadron enters a single hard scattering. Each is accompanied only by extra gluons of the longitudinal polarization that can be reorganized by Ward identities into gauge-invariant parton densities. Also the soft subgraph at leading power only connects to the collinear subgraphs and by gluons.

It is possible for the single hard scattering to produce, in addition to the lepton pair, one or more extra partons of high transverse momentum, Fig. 5.19. These manifest themselves as jets in the hadronic final state, just as in the corresponding situation for e^+e^- annihilation or DIS.

If instead we restrict to a minimal reduced graph, and then multiply by the complex conjugate amplitude, we get the cut graph shown in Fig. 5.20. This is the natural

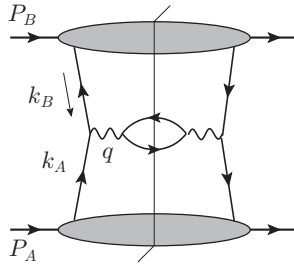


Fig. 5.20. Minimal reduced graph for cross section for the Drell-Yan process.

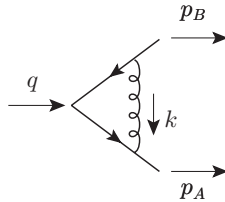


Fig. 5.21. One-loop vertex graph.

generalization of the corresponding structure that led to the parton model in DIS, Fig. 2.5(b). The most elementary treatment of this situation leads to the parton model formula for lepton-pair production, first worked out by Drell and Yan (1970). Here the lepton pair is produced in the lowest-order annihilation of a quark out of one hadron, and an antiquark out of the other, with the same parton densities as in DIS.

We thus see a general pattern: Libby and Sterman’s insight leads to the reduced diagram analysis. Approximating the situation by configurations corresponding to the simplest reduced graphs gives us the parton model, with the natural space-time interpretation. The general reduced graph plus the restriction to leading power delimits the maximum way in which we have to distort the parton model to get the results of real QCD.

5.4 One-loop vertex graph

To illustrate the properties of the regions associated with PSSs, we examine the PSSs for the one-loop vertex graph of Fig. 5.21:

$$G_1 = \frac{ig^2}{(2\pi)^n} \int d^n k \frac{\text{numerator}}{(k^2 - m_g^2 + i0)[(p_A - k)^2 - m_q^2 + i0][(p_B + k)^2 - m_q^2 + i0]}. \tag{5.17}$$

The numerator factor is irrelevant for determining the positions of the PSSs. But it is important in computing their strengths, for which different field theory models give interesting characteristic effects. We also allow a gluon mass, which is zero in QCD, but not necessarily

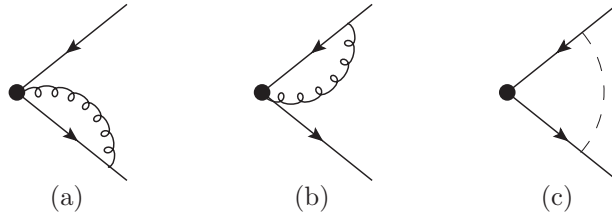


Fig. 5.22. Reduced graphs for PSSs R_A , R_B , and R_S of Fig. 5.21. The dot represents the short-distance reduced graph, the diagonal lines are collinear in the appropriate directions, and the dashed line is soft (zero momentum).

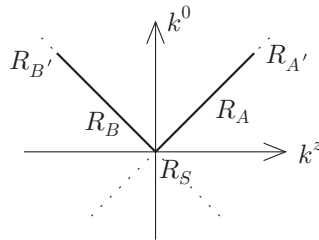


Fig. 5.23. Location of massless PSSs of Fig. 5.21 in the space of the gluon momentum. The singularities are all in the plane of zero transverse momentum, so we just show the plane of k^0 and k^z , with the $2 - 2\epsilon$ transverse dimensions out of the paper.

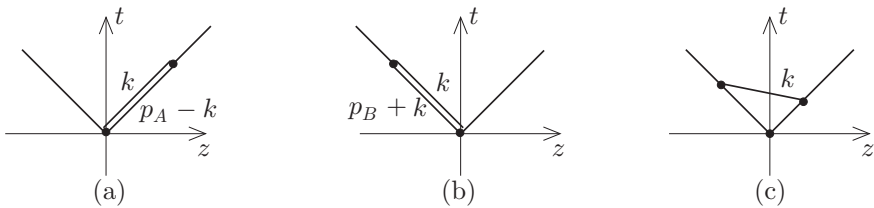


Fig. 5.24. Space-time description of PSSs of Fig. 5.22. For all three plots, the scale for the separation of the vertices is Q/λ^2 , where λ is the radial integration variable in (5.29) for a collinear region, but λ^2/Q is the radial variable in (5.49) for the soft region.

in other model theories. Generally, I will assume that the external quark lines are on-shell, equipped with Dirac wave functions as appropriate.

5.4.1 Geometry and topology of PSSs

Useful insights are obtained from each of several ways of examining the PSSs: in terms of reduced graphs (Fig. 5.22), in terms of PSSs' locations in the space of loop momenta (Fig. 5.23), and in terms of the locations of the graph's vertices in space-time (Fig. 5.24).

The criterion, of a classically allowed process in the massless limit, gives the following PSSs, which I label by the nature of the gluon’s momentum, (R_A , R_B , etc.³):

1. **Gluon collinear to A:** We label this PSS R_A . It has two massless on-shell lines: k and $p_{A,\infty} - k$, each parallel to $p_{A,\infty}$:

$$R_A : \begin{cases} k = zp_{A,\infty}, \\ p_{A,\infty} - k = (1 - z)p_{A,\infty}, \end{cases} \quad (5.18)$$

with z between 0 and 1. The line $p_B + k$ has virtuality of order Q^2 : $(p_{B,\infty} + k)^2 = Q^2z$.

In the reduced graph, Fig. 5.22(a), the far off-shell line $p_B + k$ is contracted with the current vertex to form a composite reduced vertex. Out of this come two massless on-shell momenta in the $p_{A,\infty}$ direction, which later combine to make a single massless on-shell momentum $p_{A,\infty}$.

The momentum fraction variable z must be between 0 and 1, since other values of z do not give a classical scattering configuration. For example, if z is negative, the quark goes out to the future from the current vertex, but the gluon comes in from the past. Thus they are unable to meet at the recombination point if $z < 0$.

2. **Gluon collinear to B:** This PSS, labeled R_B , with reduced graph Fig. 5.22(b), is exactly like the first PSS, but with the roles of the quark lines exchanged:

$$R_B : \begin{cases} -k = zp_{B,\infty}, \\ p_{B,\infty} + k = (1 - z)p_{B,\infty}. \end{cases} \quad (5.19)$$

3. **Soft gluon:** k has zero momentum on this PSS, which we call R_S . Its reduced graph is Fig. 5.22(c), and the quark lines have massless momenta $p_{A,\infty}$ and $p_{B,\infty}$. The quark and antiquark come out of the electromagnetic vertex and a soft gluon is exchanged. This is a rather special case of the Landau-Coleman-Norton criterion.
4. **Soft quark:** Here it is the internal quark instead of the gluon that is soft. Since the gluon now has a maximal collinear momentum $k = p_{A,\infty}$, we label this region $R_{A'}$.
5. **Soft antiquark:** Here the internal antiquark is soft, and the gluon has $k = -p_{B,\infty}$. The PSS’s label is $R_{B'}$.

The locations of the PSSs in loop-momentum space are shown in Fig. 5.23, from which can be seen some topological relations between the different PSSs. For example, R_S is at the intersection of R_A and R_B , while $R_{A'}$ is an endpoint of R_A . When we derive factorization theorems, we will find contributions and approximations associated with each PSS. The topological relations between different PSSs will determine subtractions that prevent double counting between different contributions. There will also be a contribution from the region R_H where all internal lines are far off-shell. We therefore will speak about regions; intuitively a region connotes a particular part of loop-momentum space. But as a precise mathematical notion we will use the PSSs supplemented by the hard region R_H . The intuitive notion of a region means, roughly, momenta near the corresponding PSS.

³ The subscripts should not be confused with the same symbols used to denote the various subgraphs of a reduced graph.

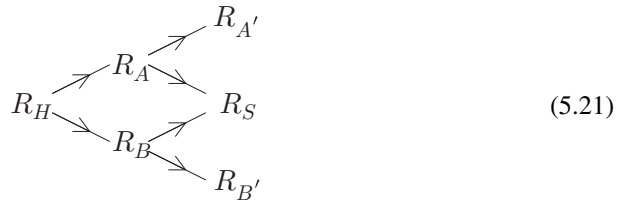
To formalize the relations between regions we first define a manifold for each PSS:

Name	Manifold	Dimension
R_S	$\{k = 0\}$	0
$R_{A'}$	$\{k = p_{A,\infty}\}$	0
$R_{B'}$	$\{k = -p_{B,\infty}\}$	0
R_A	$\{k = zp_{A,\infty} : 0 < z < 1\}$	1
R_B	$\{k = -zp_{B,\infty} : 0 < z < 1\}$	1
R_H	$\{\text{all } k \text{ such that } k \notin R_A, R_B, R_S, R_{A'}, R_{B'}\}$	4

(5.20)

Each manifold *excludes* the manifolds for smaller PSSs. For example, in the regions R_A and R_B we exclude the point $z = 0$, i.e., $k = 0$, since this does not give a collinear gluon momentum.

There is evidently a hierarchy of sizes of region:



where the biggest region is on the left. A formal definition of the hierarchy is not by simple set-theoretic inclusion, since the manifolds for smaller regions are not part of those for the bigger ones. Instead we define the hierarchy in terms of the topological closures \bar{R} of the manifolds R for the various regions. For example, $\bar{R}_A = \{k = zp_{A,\infty} : 0 \leq z \leq 1\}$, with the endpoints at $z = 0$ and $z = 1$ included. Then we define the statement that a PSS R_1 is bigger than a PSS R_2 , $R_1 > R_2$, to mean that $\bar{R}_1 \supset \bar{R}_2$.

For the actual graph with massive propagators, and possibly off-shell external quarks, we have already argued that there are important contributions from momenta close to the PSSs. This suggests a coordinate-space interpretation in terms of the relative positions of the vertices. For example, near the PSS R_A , the upper quark line $p_B + k$ has virtuality of order Q^2 , and therefore the vertices at its ends are separated by order $1/Q$. The other two lines, k and $p_A - k$, have low virtuality, so the invariant separation of their ends is much larger than $1/Q$. Moreover, the lines are highly boosted in the $+z$ direction. This gives typical locations for the vertices as shown in Fig. 5.24(a), which corresponds closely to the classical scattering picture given by the Coleman-Norton criterion. Corresponding situations for the PSSs R_B and R_S are also shown in Fig. 5.24(b) and (c). The arguments just given are quite heuristic, and it is left as an exercise to derive them more formally (problem 5.1).

5.4.2 Pinch- and non-pinch-singular surfaces: collinear-to-A

PSS R_A was restricted to $k = zp_{A,\infty}$ with z between 0 and 1. But the massless limit of the integrand in (5.17) is singular for any value of z ; it is the criterion of a pinch that restricts z ,

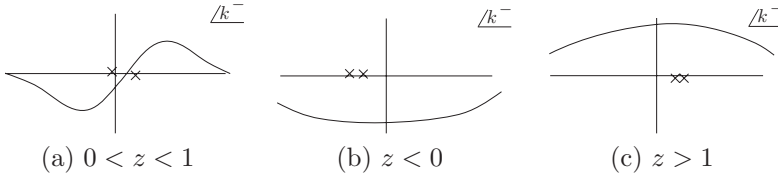


Fig. 5.25. The k^- plane, showing the singularities for the lines k and $p_A - k$ for the three cases $0 < z < 1$, $z < 0$, and $z > 1$, together with appropriate choices of contour. The scale of the diagram is roughly $(k_T^2 + m^2)/p_A^+$; the pole for the $p_B + k$ line is far off-scale, at $k^- = -O(Q^2/p_A^+)$.

as we now verify explicitly. We use light-front coordinates, as is natural for collinear PSSs, to give

$$G_1 = \frac{ig^2}{(2\pi)^n} \int d^n k \frac{\text{numerator}}{[2(p_B^- + k^-)(zp_A^+ + p_B^+) - k_T^2 - m_q^2 + i0]} \times \frac{1}{(2zp_A^+k^- - k_T^2 - m_g^2 + i0) [2(1 - z)p_A^+(p_A^- - k^-) - k_T^2 - m_q^2 + i0]}. \quad (5.22)$$

Here we wrote $k^+ = zp_A^+$, so that $d^n k = dz p_A^+ dk^- d^{n-2}k_T$.

In the following discussion, there are order-of-magnitude estimates for denominators, and it is convenient to use the symbol m as a generic size for all masses in the problem.

To understand the R_A region, we choose k_T to be much less than Q , and we examine the contour integral for k^- . In the center-of-mass frame, the large components of external momenta are p_A^+ and p_B^- , of order Q , while the small components, p_A^- and p_B^+ , are of order m^2/Q . The poles on the collinear lines k and $p_A - k$ are at small values of $|k^-|$, of order $(k_T^2 + m^2)/Q$, and, when $0 < z < 1$, they are on opposite sides of the real axis, trapping the contour, as in Fig. 5.25(a). In contrast, the remaining pole, from the $p_B + k$ line, is much further away, at $k^- \simeq -p_B^- = -O(Q)$, corresponding to the line's large virtuality in the R_A region.

Naturally, when z approaches 0 or 1, the accuracy of this argument degrades. For example, the separation of the poles in k^- is of order

$$\frac{k_T^2 + m^2}{p_A^+} \left(\frac{1}{z} + \frac{1}{1 - z} \right), \quad (5.23)$$

and this gets large close to the endpoints of R_A , i.e., near the R_S and $R_{A'}$ regions. This formula also exhibits the exact pinch in the massless limit. That is, when $m = 0$, the minimum distance between the poles is zero, obtained at $k_T = 0$.

Outside the PSS region, i.e., for z below 0 or above 1, the two collinear denominators are on the same side of the real axis: Fig. 5.25(b) and (c). Then we can deform k^- to be of order Q , so that all the denominators are of order Q^2 , i.e., the momenta are in the hard region. Note that we cannot deform the contour all the way to infinity, to give a zero integral, because of the singularity on the $p_B + k$ line.

5.4.3 Multidimensional contour deformation

For one variable, like k^- , the analysis of the pinch condition is straightforward, because the contour deformation is visualizable. But the actual integral is multidimensional, and thus hard to visualize. Is there a cunning deformation of the contour in z and/or k_T that would allow the four-complex-dimensional⁴ contour to avoid the poles? The Landau criterion asserts in complete generality that this cannot be done.

A devil's advocate would search for a proof in the literature that the Landau equations are both necessary and sufficient for a PSS, and would be rewarded by *not* finding a published explicit and complete proof. Textbook treatments, when examined closely, are incomplete. For example, in the authoritative book on analyticity properties in QFT, by Eden *et al.* (1966), we read (p. 48): "A proper proof needs the use of topology; . . . We shall be content with plausibility arguments." The reference given for a real proof is an *unpublished* paper, by Fotiadis, Froissart, Lascoux, and Pham; the paper, as far as I can find out, is still unpublished forty years later. Devil's advocates are recommended to investigate further (problem 5.3); there is something in this subject that is not fully understood.

I now present some techniques to help formalize issues about contour deformation in the general case, with the momentum integral for L loops having nL dimensions. The aim is to make very transparent the concepts that relate exact PSSs in the massless theory to properties of actual integrals with non-zero masses but large Q .

First we write the loop momentum in terms of real and imaginary parts:

$$k = k_R + i\kappa k_I(k_R). \quad (5.24)$$

Here a contour deformation is characterized by increasing the real parameter κ from 0 to 1, with each point on the contour labeled by its (nL -dimensional) real part k_R . The imaginary part is some function of the real part, and naturally $d^{nL}k$ includes a Jacobian for the transformation between k and k_R . An allowed contour deformation is one for which no poles are crossed in going from $\kappa = 0$ to $\kappa = 1$. We also require a uniform upper bound on the derivatives $\partial k_{Ia}/\partial k_{Rb}$, so that the Jacobian stays finite; otherwise, an arbitrarily large size for Jacobian would ruin our derivation of power-counting. Thus in a one-dimensional contour integral we might require the deformed contour to have an angle of at most 45° to the real axis. The precise bound does not matter, but having an angle close to 90° would give a very big Jacobian.

Next consider a denominator $D(k) + i0$ at a zero of $D(k)$. Our aim is to determine whether this denominator participates in a pinch at this value of momentum, or whether the contour of k can be deformed away. We avoid the corresponding pole if D acquires a positive imaginary part when κ becomes slightly positive, i.e., if

$$k_I \cdot \frac{\partial D}{\partial k} > 0 \quad \text{pole avoidance criterion} \quad (5.25)$$

at the zero of D . We have an exact pinch if, no matter what choice we make for k_I , (5.25) fails for at least one of the on-shell lines.

⁴ Or $4 - 2\epsilon$ -dimensional contour.

The criterion just stated applies to determining whether there is an exact pinch. In our context, the PSSs we are cataloging are those of the massless theory. But our use of these PSSs is also in the massive theory, where we are concerned not with whether or not there is an exact pinch, but with whether or not the integration contour is forced to be close to particular propagator poles. So we now ask: What are the appropriate criteria for avoiding or not avoiding poles in the massive theory?

We do not consider a particular pole to be avoided unless the minimum value of $|D(k)|$ on the deformed contour is of order Q^2 in a whole neighborhood of some candidate for a PSS. The neighborhood should be of a size of order Q in the components of loop momentum k_R . Now all the momentum components of interest are at most of order Q , and similarly for the derivatives $\partial D/\partial k$. For the denominator to be of order Q^2 when the real part of k is at a zero of $D(k)$, it must be true that the imaginary part has a component of order Q .

It also follows that the first-order term in an expansion in powers of k_I , i.e., the l.h.s. of (5.25), must itself be of order Q^2 . Otherwise the first derivative would change sign near our initially chosen k_R , since the second derivative is of order unity, and then we would find places where, as we deform the contour, the denominator gets a negative imaginary part. Because of the limit on the gradient of k_I with respect to k_R , the pole avoidance condition (5.25) is obeyed, not just exactly at the PSS, but in a neighborhood. It also follows that the component of $\partial D/\partial k$ in the direction k_I is of order Q .

In the example of the two collinear denominators for region R_A of the vertex graph, the derivatives are

$$\frac{\partial(k^2 - m_g^2)}{\partial k} = 2k \simeq 2z p_{A,\infty}, \quad \frac{\partial((p_A - k)^2 - m^2)}{\partial k} \simeq -2(1 - z)p_{A,\infty}. \quad (5.26)$$

On PSS R_A , these two vectors are opposite in direction, so that the pole avoidance criterion (5.25) cannot be simultaneously satisfied by both denominators. The exact PSS is in the massless theory, but small changes in the pole positions, to allow for masses, do not break this argument. As just explained, any contour deformation that successfully avoids a singularity has to work over a large neighborhood of the propagator poles. If we tried deforming another component of k than k^- , its imaginary part would multiply a small derivative on the l.h.s. of (5.25), and would not make this l.h.s. of order Q^2 .

In contrast, when we extrapolate the PSS to $z < 0$ or to $z > 1$, the two derivative vectors have the same direction. Therefore if we choose k_I to give one denominator a large positive imaginary part, then the other denominator also gets an imaginary part of the same sign. Thus we can avoid the pole. Since $k_I \cdot p_{A,\infty} = k_I^- p_{A,\infty}^+$, it is the minus component of k_I that needs to be made large to avoid the pole; this again justifies our choice to examine contour integration only over k^- . Therefore the singular surfaces at $z < 0$ and $z > 1$ are not PSSs.

5.5 Power-counting for vertex graph

I next use the one-loop vertex graph to motivate the primary tools for power-counting. In addition, we will encounter the so-called Glauber region of gluon momenta. Glauber

momenta form a subset of soft momenta, but require a different treatment than generic soft momenta; in particular standard factorization is only obtained after a contour deformation away from momenta in the Glauber region.

For the power-counting, I will usually set the space-time dimension to $n = 4$. But to discuss properties of regulated integrals, I will sometimes change to $n = 4 - 2\epsilon$.

Characteristic differences between QFTs are controlled by the numerator factor in (5.17), and we can see the spectrum of possibilities from specific examples:

- A ϕ^3 -type theory where both the quarks and gluons are scalar fields, and the vertex for the electromagnetic current is replaced by one for a ϕ^2 operator. It gives a numerator factor of unity.
- A Yukawa theory with a scalar “gluon” and fermionic quarks. It gives a numerator $\bar{u}_A [\gamma \cdot (p_A - k) + m_q] \gamma^\mu [- \gamma \cdot (p_B + k) + m_q] v_B$, where u_A and v_B are Dirac wave functions.
- A gauge theory with fermion quarks. The numerator factor is

$$\bar{u}_A \gamma^\kappa [\gamma \cdot (p_A - k) + m_q] \gamma^\mu [- \gamma \cdot (p_B + k) + m_q] \gamma^\lambda v_B N_{\kappa\lambda}. \tag{5.27}$$

In Feynman gauge, the gluon part of numerator is $N_{\kappa\lambda} = -g_{\kappa\lambda}$.

(Further cases are left as an exercise; problem 5.6.) In addition, we will examine how the power laws change with the dimension of space-time.

Our main interest is in the size and power law of the loop graph *relative to the lowest-order* graph. For the ϕ^3 theory, the lowest-order graph is unity, but for the other two theories, the lowest-order graph is of order Q , since the largest component of a Dirac wave function grows like $Q^{1/2}$.

5.5.1 Hard region R_H : power corresponds to UV divergence

In region R_H , all momentum components are of order Q and all virtualities are of order Q^2 . As we found around (5.6), the power of Q is given by dimensional analysis, and is the same as for UV divergences. Thus in ϕ^3 theory at $n = 4$, region R_H ’s contribution to the vertex graph is of order $1/Q^2$. In Yukawa and gauge theories, which are renormalizable, the numerators provide factors of Q^2 times Dirac wave functions, so the contribution is of the same power as the lowest-order vertex, and we call R_H a leading region. Of course, if we increased the space-time dimension to 6 in ϕ^3 theory we also get leading behavior. These arguments apply after UV renormalization, provided we apply an RG transformation to set the renormalization scale μ of order Q .

In any of the renormalizable theories, we therefore write the contribution of region R_H as

$$G_1 \text{ in } R_H = O(1) \times \text{LO}. \tag{5.28}$$

This simply means that we have a bound. That is, for large Q/m , the size of this contribution is less than some constant number times the lowest-order graph. In QCD (for example), a useful bound is the product of

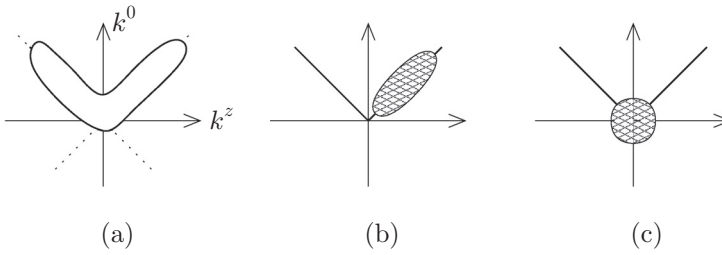


Fig. 5.26. (a) Integration domain used for region H ; it excludes the blanked-out area around the PSSs. The size of the regions shown is a modest factor less than Q . This diagram should be treated as having two more dimensions perpendicular to the ones shown. (b) Integration domain used for region A , the cross-hatched area. (c) Integration domain used for region S .

- a factor of a few, from the approximations on the denominators and from the multiple terms in the Dirac algebra;
- a factor $g^2/(16\pi^4)$ explicitly in the Feynman rules; and
- π^2 from an angular integral in four space-time dimensions.

This gives a modest factor times $g^2/16\pi^2$. In principle there could be cancellations, since the sign and complex phase of the integrand are not fixed. But, in general, if such cancellations occur frequently and are strong, we should expect this to have a specific cause.

The integration domain for an actual numerical estimate should be like that in Fig. 5.26(a). Here we cut out pieces surrounding each of the (smaller) PSSs, perhaps of size $Q/2$. The precise positions of the borders will not bother us. But we must insist that a contour deformation is applied to stay away from all propagator poles where there is not a PSS. For example, suppose k is close to a *negative* number times $p_{A,\infty}$. Without the contour deformation, we would have two low-virtuality denominators, which falsifies the derivation of the estimate. A convenient way of interpreting Fig. 5.26(a) is to treat the variables plotted there as the real parts k_R . Imaginary parts, as in (5.24), give denominators of order Q^2 , for example from the contour deformation in Fig. 5.25(b).

5.5.2 Basic treatment of collinear region R_A

Next we integrate around the PSS for region R_A , Fig. 5.26(b), excluding neighborhoods of the smaller PSSs, R_S and $R_{A'}$. The dimensionless variable z parameterizes the PSS; we call it an intrinsic variable for the PSS. At fixed z , consider the integral over k^- and k_T , which parameterize the deviation from the PSS, and which we therefore term normal variables for the PSS. Near the PSS the momentum $p_B + k$ is off-shell by approximately zQ^2 . On the other hand, the momenta k and $p_A - k$, which we call collinear, are approximately parallel to p_A .

To understand the integral's behavior near the PSS as an example of a general case, we change to a set of dimensionless variables \bar{k} parameterizing a surface surrounding the PSS, together with a radial variable λ with the units of mass that scales this surface and is chosen

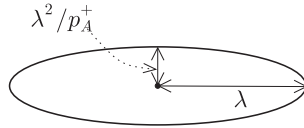


Fig. 5.27. Surface of fixed λ surrounding a collinear PSS. The surface is drawn asymmetrically, to correspond to the scalings defined in (5.29).

to lie in the range $0 \leq \lambda \leq Q$. Observe that the collinear denominators are quadratic in k_T but linear in k^- . So we choose different scalings for k^- and k_T :

$$\text{Collinear to A: } k^- = \lambda^2 \bar{k}^- / p_A^+, \quad k_T = \lambda \bar{k}_T, \tag{5.29}$$

as illustrated in Fig. 5.27. These variables should be thought of as generalized polar coordinates, with \bar{k} being treated as two-dimensional angular variables. The definition is non-unique, and we can specify it by giving λ as a function of k^- and k_T :

$$\lambda = f(|k^-|, |k_T|, p_A^+), \tag{5.30}$$

of a form consistent with the scaling law (5.29). I choose

$$f(|k^-|, |k_T|, p_A^+) = \sqrt{|p_A^+ k^-| + |k_T|^2}. \tag{5.31}$$

Such a definition is not Lorentz invariant, but is intended to be applied in a natural frame for the process, which is the center of mass. I have arranged for the definition to be invariant under z boosts, and for the angular variables \bar{k}^- and \bar{k}_T to be dimensionless. Given (5.29) and (5.31), the angular variables satisfy the normalization condition $|\bar{k}^-| + |\bar{k}_T|^2 = 1$.

To understand the size of the integrand, and the consequent power-counting, we examine the dependence on λ . In each collinear denominator there are terms of order λ^2 and of order m^2 , e.g., $-\lambda^2 \times 2(1-z)\bar{k}^- - \lambda^2 \bar{k}_T^2 + p_A^2(1-z) - m^2$ for $p_A - k$. Since the angular variables parameterize a (two-dimensional) surface surrounding a point on the PSS, they cover over a finite range independent of λ , and only one of $p_A^+ \bar{k}^-$ and \bar{k}_T can go to zero simultaneously. Thus in estimating sizes, we write the collinear denominators as $\lambda^2 O(1) + m^2 O(1)$, where “ $O(1)$ ” denotes a quantity that goes over a finite range, never approaching infinity.

However, this is not sufficient to obtain a result for the integral. The problem is that the argument so far only gives us an upper bound on the denominators, and the denominators can and do get arbitrarily small. Thus for the integral itself we cannot directly deduce an upper bound. But we can limit the closest approach to the poles by applying a contour deformation like that in Fig. 5.25(a), where the separation of the poles is given by (5.23). On the deformed contour there is a minimum size for each denominator, and a minimum size for k^- , for a given value of k_T .

Now the definition of λ in (5.30) was deliberately written with absolute values of the momentum components. Thus it can be applied on the deformed contour, and the integration over the purely real-valued radial variable λ can be regarded as a slicing of the k integral. We now find that on the deformed contour we can always treat the denominator as being

of order $\lambda^2 + m^2$, but in a much stricter sense. The size of each collinear denominator obeys $C_1(\lambda^2 + m^2) < |\text{denom.}| < C_2(\lambda^2 + m^2)$, where C_1 and C_2 are two constants with C_1 strictly non-zero and C_2 finite. These bounds apply uniformly for all values of \bar{k} on the contour and for all relevant values of λ . We could use separate bounds for the λ^2 and m^2 terms, but we would not gain anything useful.

There is in fact a notation for this which has become standard in some areas, and which is defined in App. A.17:

$$|\text{collinear denominator}| = \Theta(\lambda^2 + m^2). \tag{5.32}$$

The use of $\Theta(\lambda^2 + m^2)$ instead of $O(\lambda^2 + m^2)$ indicates that we have a lower as well as an upper bound, so that we can deduce a similar result also for the inverse

$$\left| \frac{1}{\text{collinear denominator}} \right| = \Theta\left(\frac{1}{\lambda^2 + m^2}\right). \tag{5.33}$$

This lets us obtain the power law associated with the R_A region. We have the following sizes, in the sense of the Θ notation:

- $1/Q^2$ for the far off-shell denominator;
- $d\lambda \lambda^3$ for the radial integration;
- $1/(\lambda^2 + m^2)$ for each of the two collinear denominators;
- unity for the integral over the angular variables \bar{k} ;
- a numerator factor.

First, we ignore the numerator, and provide an estimate for the ϕ^3 theory:

$$R_A \text{ region} = \frac{g^2}{Q^2} \int_0^Q \frac{d\lambda \lambda^3}{\Theta(\lambda^2 + m^2)^2} \tag{5.34}$$

$$= O\left(\frac{g^2 \ln(Q^2/m^2)}{Q^2}\right). \tag{5.35}$$

Since the integrand has a variable complex phase, there is a possibility of a cancellation, so that we must use the symbol $O(\dots)$ rather than $\Theta(\dots)$ for our estimate of the integral.

From (5.34), we see that for *large* λ , of order Q , the estimate matches our result $1/Q^2$ for the hard region R_H in ϕ^3 theory. For small λ , when m is set to zero, we get a logarithmic (collinear) divergence at $\lambda = 0$, i.e., the degree of collinear divergence is zero. This symptomizes two properties of the actual massive integral: (a) for λ of order m , we get the same size as in the hard region R_H ; (b) there there is a logarithmic enhancement from the region $m \ll \lambda \ll Q$. This is an example of a general result, that if the two regions have the same power law, then there is a logarithmic enhancement from the integral between the extremes, with the exponent of the power being unchanged.

If we change the space-time dimension from 4 to n , the power for $\lambda \sim m$ is changed to $g^2 m^{n-4}/Q^2$. Thus in ϕ^3 theory, i.e., without the numerator factor, the collinear region always has a $1/Q^2$ suppression independent of space-time dimension; i.e., this region is never leading. There is a contribution from the hard region of order $g^2 Q^{n-6}$.

5.5.3 Where are the vertices in space-time?

We did not associate the space-time picture of a classical space-time process at a PSS with any specific distance scale. We now remedy this defect. The argument is sketchy, and making a more detailed argument is left for problem 5.1.

It is reasonable that the typical time between two ends of a line of a Feynman graph is the inverse of the deviation of its energy from being on-shell:

$$\Delta t \sim \frac{1}{|k^0 - E_k|} = \frac{|k^0 + E_k|}{|k^2 - m^2|} \sim \frac{E_k}{|k^2 - m^2|}. \quad (5.36)$$

Naturally, we assume that the integration contour has been deformed as far away as possible from propagator poles.

For a collinear line, with its momentum scaled as in (5.29), we find a time of order Q/λ^2 . This can be interpreted as a time $1/\lambda$ in the rest-frame of the collinear system multiplied by a time-dilation factor Q/λ . The boost argument shows that this is also the separation of the vertices in x^+ , and that the separation in the other light-front coordinate x^- is of order $1/Q$, the same as the size of the hard scattering. The separation in transverse position is invariant under a boost in the z direction, and is therefore $1/\lambda$.

This therefore gives a scale for the drawings in Figs. 5.24(a) and (b), and for their generalizations to higher-order graphs.

One caveat is needed. When λ becomes less than the quark and gluon masses, the virtuality of the lines remains of order m^2 instead of scaling down like λ^2 , so we should really equip the estimate with a minimum:

$$\Delta t \sim \frac{Q}{\max(\lambda^2, m^2)}, \quad (5.37)$$

from the pole separation value given in (5.23). Naturally, if both the quark and gluon have zero mass, then the time scale goes to infinity as λ goes to zero; this corresponds to the actual collinear divergence in the massless case.

5.5.4 Collinear region boosted from rest frame

We now consider a general case of a collinear subgraph, and more generally a non-perturbative amplitude for a collinear subgraph, as in the lower bubble in Fig. 2.5(b) for the parton model for DIS. We can regard a collinear subgraph or amplitude as being obtained by a boost from its rest frame. We always define a collinear subgraph to include all its attached collinear lines and the integral over all the small components of the collinear momenta.

For scalar fields, a collinear subgraph is boost invariant. Thus the collinear subgraph counts as Q^0 , and the power law for the whole graph is just that for the hard part of the graph, i.e., $1/Q^2$ in our one-loop example, independent of the space-time dimension.

For a field with spin s , the biggest component of a matrix element of its field grows like $(Q/m)^s$ under a boost to energy of order Q from a rest frame associated with mass m . This

gives enhancements that we now investigate. We will find them to be particularly notable for the exchange of a field of the highest spin, i.e., for the gluon.

5.5.5 Yukawa theory, region R_A

First we examine the on-shell electromagnetic vertex of a fermion in Yukawa theory. The Dirac wave functions for a spin- $\frac{1}{2}$ fermion grows like $Q^{1/2}$ in the center-of-mass frame, so the tree-graph amplitude grows like Q .

For the one-loop graph in the Yukawa theory in a collinear region, the boost argument of Sec. 5.5.4 shows that the same $Q^{1/2}$ growth applies to the whole collinear subgraph (lines k and $p_A - k$) as to the Dirac wave function. Thus the power of Q for the whole graph in the R_A region is given by the off-shell propagator $i[-\gamma \cdot (p_B + k) + m]/[(p_B + k)^2 - m^2]$. This now has dimension -1 , so it contributes $1/Q$, and we get a power suppression.

From the overall numerator factor, $[\gamma \cdot (p_A - k) + m_q] \gamma^\mu [-\gamma \cdot (p_B + k) + m_q]$, this is not quite so obvious, since it contains two factors with momentum components of order Q . These might compensate the $1/Q^2$ suppression from the $p_B + k$ denominator. But the large part of the $p_A - k$ numerator can be eliminated by the equations of motion for a Dirac spinor:

$$\bar{u}_A \gamma^- (p_A^+ - k^+) = (1 - z) \bar{u}_A \gamma^- p_A^+ = (1 - z) \bar{u}_A (m - \gamma^+ p_A^-). \tag{5.38}$$

The boost argument shows that this is part of a general result, not an accident of a one-loop calculation.

5.5.6 Gauge theory, region R_A

The situation changes when the exchanged line is for a vector field, as in QCD. The collinear part of the graph is proportional to

$$\int d^4k \frac{\bar{u}_A \gamma^\kappa [\gamma \cdot (p_A - k) + m_q] \gamma^\mu}{(k^2 - m_g^2 + i0) [(p_A - k)^2 - m_q^2 + i0]}. \tag{5.39}$$

Under a boost, the $\kappa = +$ component gains a factor of order Q relative to the size in a Yukawa theory; this removes the $1/Q$ suppression from the off-shell $p_B + k$ line. The gluon collinear region is therefore leading, independently of the space-time dimension. The same leading power applies to any graph in which arbitrarily many gluons go from a collinear subgraph to a hard subgraph. This immediately implies that substantial modifications are needed to the derivation of even the elementary parton model. Instead of considering graphs like Fig. 2.5(b), we must allow extra gluon exchanges to the hard subgraph, as in Fig. 5.7(c).

The resulting complications are tamed, as we will see in later chapters, by noticing that the enhancement is associated with the one component, $\kappa = +$, of the gluon field that scales like Q/m under the boost to the collinear-to- A direction. In (5.27), the dominant part of the gluon numerator is N_{+-} . This dominance can be eliminated by a gauge transformation,

e.g., by a suitable choice of axial gauge $n \cdot A = 0$, for which the gluon numerator is

$$N_{\kappa\lambda}^{\text{axial-gauge}} = -g_{\kappa\lambda} + \frac{k_\kappa n_\lambda + n_\kappa k_\lambda}{k \cdot n} - \frac{k_\kappa k_\lambda n^2}{(k \cdot n)^2}. \tag{5.40}$$

If we choose n at rest in the center-of-mass, say $n \propto p_A + p_B$, the all-important N_{+-} component is $-k^- k^+ n^2 / (k \cdot n)^2$. It is readily checked that when k is a collinear momentum, this is of order m^2 / Q^2 ; the contribution of region R_A in this gauge is thus suppressed by two powers of Q .

Another common choice is the light-front gauge: $n \cdot A = A^+ = 0$; in that case N_{+-} is exactly zero. However, this gauge is not symmetric between p_A and p_B , so that it causes difficulties in a general treatment. Even the non-light-like case, with $n^2 \neq 0$, is not adequate for our later work, because the singularity at $k \cdot n = 0$ breaks standard analyticity rules for propagators that are needed in proofs of factorization; see Ch. 14.

Therefore we will generally stay in the Feynman gauge, with the implication that regions with collinear gluon exchange, such as region R_A , will be leading. However, the fact that these regions can be made non-leading by a certain choice of gauge, implies that important simplifications can be made by the use of Ward identities.

We can see the basic idea of the argument by the following chain of approximations for the numerator. We consider a general situation in which one gluon connects a collinear-to- A subgraph to a hard subgraph:

$$\begin{aligned} \text{collinear-}A^\kappa N_{\kappa\lambda} \text{ hard}^\lambda &\simeq \text{collinear-}A^\kappa N_{\kappa-} \text{ hard}^- \\ &= \text{collinear-}A^\kappa N_{\kappa-} \frac{1}{k^+} k^+ \text{ hard}^- \\ &\simeq \text{collinear-}A^\kappa N_{\kappa-} \frac{1}{k^+} k \cdot \text{ hard}. \end{aligned} \tag{5.41}$$

All the approximations are accurate at the leading power of Q . In the first line, we replaced the hard subgraph by its minus component, that dominates in the contraction with the collinear-to- A subgraph. Then we multiplied and divided by k^+ , which allows us in the last line to replace $k^+ \dots$ by $k \cdot \dots$ for the gluon connecting to the hard scattering, accurate to the leading power of Q . Having k contracted with the hard subgraph is exactly of the form to which a Ward identity applies. This method was obtained by generalizing the argument of Grammer and Yennie (1973) that was devised for treating IR divergences in QED.

5.5.7 Effect of different degree of divergence

The above calculations exhibit some quite general phenomena in the estimation of the sizes of the contributions of different regions. For each PSS, we parameterize the approach to the PSS by a radial variable λ . The general structure of the momentum-space integrands for Feynman graphs is of products of very simple rational functions. This generally gives a power-law behavior in λ as $\lambda \rightarrow 0$, with a cutoff provided by masses.

Because the power-law dependence gives useful order-of-magnitude estimates all the way from $\lambda = 0$ to $\lambda = Q$, we can now obtain some interesting relations between the power law for different regions. The basic general form of the size of the contribution from a

region is

$$\frac{1}{Q^\alpha} \int_0^Q \frac{d\lambda \lambda^\beta}{\Theta(\lambda^2 + m^2)^\gamma}, \tag{5.42}$$

where we now allow general exponents. Situations with nested leading regions often require us to modify these estimates by logarithmic corrections from integrals over the angular variables, but this will not change the basic power laws and exponents. See p. 115 for an explanation of the Θ notation.

For order-of-magnitude estimates we have a power-law integral $d\lambda \lambda^{\beta-2\gamma}$ cutoff at the lower end by mass effects. Let us define the infra-red degree of divergence in the massless limit by $\Delta = 2\gamma - \beta - 1$.

A common, but not universal, situation in QCD and other theories in four-dimensional space-time is that we have a logarithmic divergence, $\Delta = 0$. Then, as we have seen, the total contribution has the same power $1/Q^\alpha$ as the contribution from the hard region, i.e., from $\lambda \sim Q$, but there is a logarithmic enhancement. If the integrand is modified by a logarithm, then the number of logarithms increases by one after integration, e.g.,

$$\frac{1}{Q^\alpha} \int_0^Q \frac{d\lambda \lambda^{2\gamma-1}}{\Theta(\lambda^2 + m^2)^\gamma} \ln^\delta\left(\frac{Q}{\lambda}\right) = O\left(\frac{\ln^{\delta+1}(Q/m)}{Q^\alpha}\right). \tag{5.43}$$

In this situation all scales between m and Q are important.

In contrast, if we have a power-law divergence $\Delta > 0$, then the lower end of the integral, $\lambda \sim m$, dominates, and the power there is $1/Q^\alpha$ (times $O(1/m^\Delta)$). The power from the hard region $\lambda \sim Q$ is weaker: $1/Q^{\alpha+\Delta}$. From a UV-centric point of view, we can say that in this situation there are power-law enhancements as we go from large to small momenta. Alternatively we can take an IR-centric view: momenta near the IR scale dominate, and there is a convergent extrapolation of the integral to infinite λ . This situation is typical in a model super-renormalizable QFT in a space-time of dimension less than 4.

The reverse holds if Δ is negative. In that case the hard region $\lambda \sim Q$ dominates and we can legitimately neglect masses.

In all cases, the power law for the region for the PSS at $\lambda = 0$ is $1/Q^\alpha$ and the power for the hard region is $1/Q^{\alpha+\Delta}$, with the proviso that we may have logarithmic enhancement(s) associated with IR degree of divergence zero.

5.5.8 Soft-gluon region R_S

For the soft-gluon region R_S we integrate over a domain like that in Fig. 5.26(c) that surrounds R_S (a single point in this case). To parameterize the approach to R_S , we use the same scaling for all components of k :

$$k^\mu = \lambda_S \bar{k}^\mu. \tag{5.44}$$

Again the radial variable λ_S has the dimensions of mass and is specified by a (non-Lorentz-covariant) function

$$\lambda_S = f_S(k^\mu), \tag{5.45}$$

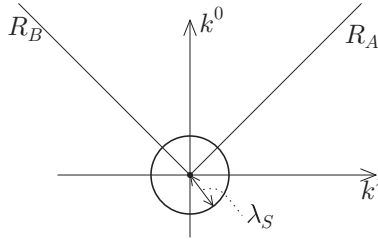


Fig. 5.28. Surface of fixed λ_S surrounding the soft PSS R_S . In contrast to the collinear case, Fig. 5.27, we have the same scaling on all components of k . The diagonal lines are the *soft ends* of the PSSs R_A and R_B .

with an appropriate scaling property. We choose

$$f_S(k^\mu) = \sum_\mu |k^\mu|. \tag{5.46}$$

(Three-dimensional) surfaces of fixed λ_S surround the point $k = 0$, which is the PSS for R_S (Fig. 5.28). From (5.46), the angular variables are normalized to $\sum_\mu |\bar{k}^\mu| = 1$.

Many interesting complications in perturbative QCD arise from soft gluons and their couplings to collinear subgraphs. One is simply that soft gluon connected to collinear subgraphs give leading-power contributions. As we will see in Sec. 5.5.10, another complication arises because soft loop momenta circulate through collinear subgraphs, so that the power-counting for λ_S depends non-trivially on properties of the collinear subgraphs and the relative sizes of the components of soft momenta.

We first derive a basic scaling argument for the integral near the PSS R_S for the one-loop vertex graph. It applies for generic values of the angular variables \bar{k} , i.e., when any considered combination of the components of \bar{k} is of order unity. Later, in Sec. 5.5.10, we will consider the relatively small Glauber region, where the argument needs to be changed. For the generic case:

1. The integration measure is $d\lambda_S \lambda_S^{n-1} d^{n-1}\bar{k}$, which gives a power λ_S^n , where n is the dimension of space-time.
2. The gluon denominator $k^2 - m_g^2$ is $\lambda_S^2 \bar{k}^2 - m_g^2$, i.e., its size is $O(\lambda_S^2 + m^2)$. In the massless limit, or when m_g is negligible, this is simply $O(\lambda_S^2)$. The gluon mass becomes important when λ_S is around m_g .
3. The lower quark denominator is

$$(p_A - k)^2 - m_q^2 = p_A^2 - m_q^2 - 2p_A \cdot \bar{k} \lambda_S + \lambda_S^2 \bar{k}^2. \tag{5.47}$$

Since we treat all the components of k as comparable, the biggest k -dependent term is $-2p_A^+ \bar{k}^- \lambda_S$, so that the denominator is $O(\lambda_S Q + m^2)$. In the massless limit, the dominant term is $-2p_A^+ \bar{k}^- \lambda_S$, i.e., $O(\lambda_S Q)$.

4. The upper antiquark denominator is treated similarly, with its dominant part in the massless limit being $2p_B^- \bar{k}^+ \lambda_S$, also $O(\lambda_S Q)$.

As regards the massless limit, this gives an overall result of order

$$\int d\lambda_S \lambda_S^{n-1} \frac{1}{\lambda_S^2} \frac{1}{(\lambda_S Q)^2} \times \text{numerator} = \int_0^{\sim Q} d\lambda_S \lambda_S^{n-5} Q^{-2} \times \text{numerator}. \quad (5.48)$$

When we set $n = 4$, the physical space-time dimension, and restore the mass cutoff, we find a logarithmic enhancement multiplying the explicit power $1/Q^2$.

The dependence on the spin of the soft line is rather interesting. The boost argument of Sec. 5.5.4 shows that the numerator gains a factor of Q^{2s} , where s is the spin of the exchanged soft line. This is an enhancement relative to the power obtained for coupling the collinear graphs to the hard subgraphs. Hence:

- For the case of both ϕ^3 and Yukawa theory, the exchanged gluon is a scalar. Therefore the explicit power $1/Q^2$ in (5.48) shows that the region R_S gives a non-leading power.
- For a vector gluon, the boost argument shows that the case $\kappa = +$ and $\lambda = -$ gives an extra factor of Q^2 . So the soft region R_S is leading, independently of the space-time dimension n .

We have now seen that in a gauge theory all of the regions R_A , R_B , and R_S for the vertex graph are of leading power. In contrast, none is leading in theories without a gauge field. The remaining regions $R_{A'}$ and $R_{B'}$ are always non-leading. In the absence of a vector field, only the hard region R_H could be leading. Hence a large number of complications in the parton physics of QCD result from QCD being a gauge theory.

5.5.9 Where are the vertices in space-time for the soft region?

Although the virtualities are different for soft and collinear lines (λ_S^2 and $\lambda_S Q$ respectively), both kinds of line give the same time scale $1/\lambda_S$ in the center-of-mass frame. This arises from time dilation of the collinear lines, and can be deduced from (5.36).

When we work with more complicated regions, it is useful for the time scale to match the one in (5.37) for the collinear region. So we define λ by $\lambda_S = \lambda^2/Q$, so that

$$\text{Soft:} \quad k^\mu = \frac{\lambda^2}{Q} \bar{k}^\mu. \quad (5.49)$$

Then the time scale is the same as for the collinear region, i.e., Q/λ^2 , to the extent that we neglect masses. It is naturally appropriate to use the λ as a redefined radial variable for the soft region.

The effect of masses is different for collinear and soft momenta. For the collinear case, masses give a lower cutoff of m on λ . For the soft region, this also applies to the *quark* mass. But the gluon mass implies a more stringent cutoff, at $\lambda \sim \sqrt{m_g Q}$. So for the soft region we replace (5.37) by

$$\Delta t \sim \frac{Q}{\max(\lambda^2, m_g Q, m^2)}. \quad (5.50)$$

Of course this makes no difference if the gluon is massless. But in real QCD there is some kind of non-perturbative infra-red cutoff due to confinement, so in real QCD physics m_g in the above equation should be replaced by Λ .

Even so, the two widely different scales of cutoff indicate that when we go to higher-order diagrams there can be complications. It will turn out that most of these will be avoided after we use Ward identities to sum over different ways of attaching soft lines to collinear subgraphs. Moreover the non-perturbative cutoff does not apply directly to Feynman graphs, so there will be some interesting issues in the leading regions and their interpretation in Feynman graphs with massless gluons and massive quarks, that will involve us with regions that are not really physical.

5.5.10 “Glauber” region

Just as with the collinear regions, there are certain parts of the integration over angular variables \vec{k} where denominators get much smaller than the estimates used above. Again we need to investigate to what extent contour deformation can rescue them, but the conclusions will now be less trivial. The necessary contour deformations work for some situations like the vertex graph, but fail for others.

This issue does not concern only the determination of the power law associated with the soft region. More importantly, it gives a danger of violating the Grammer-Yennie approximation that is essential in deriving factorization, by allowing us to apply Ward identities to the sum over soft gluon connections to collinear subgraphs. The approximation is a simple generalization of (5.41):

$$\begin{aligned} (\text{coll. } A)^{\kappa} N_{\kappa\lambda} (\text{coll. } B)^{\lambda} &\simeq (\text{coll. } A)^+ N^{-+} (\text{coll. } B)^- \\ &\simeq (\text{coll. } A) \cdot k \frac{N^{-+}}{k^+ k^-} k \cdot (\text{coll. } B). \end{aligned} \quad (5.51)$$

Here, our aim is a formula in which the gluon momentum k is contracted with each collinear factor, so that we can apply Ward identities. The critical step is in the second line, where we use the following approximations that are valid to the leading power of Q if the components of k are not too much different: $k \cdot (\text{coll. } A) \simeq k^- (\text{coll. } A)^+$ and $(\text{coll. } B) \cdot k \simeq (\text{coll. } B)^- k^+$.

When these approximations are valid, we will find that in our actual applications further approximations of k in the collinear factors are useful and valid: to replace k inside the collinear- B part by its plus component and to replace k inside the collinear- A part by its minus component.

These approximations rely on all components of k being comparable. Thus one or more of the approximations fails when k^- and/or k^+ gets too small with respect to the other components. By examining the relative sizes of components of collinear momenta, we find that the approximations are accurate under the following conditions:

$$\frac{m^2}{(p_B^-)^2} \ll \left| \frac{k^+}{k^-} \right| \ll \frac{(p_A^+)^2}{m^2}, \quad (5.52)$$

$$\left| \frac{k^+}{k_T} \right| \gg \frac{m}{p_B^-}, \quad \left| \frac{k^-}{k_T} \right| \gg \frac{m}{p_A^+}. \quad (5.53)$$

The first line simply states that the rapidity of the gluon must be well inside the range between the collinear rapidities, which is essentially the simplest definition of the soft region. The conditions on the second line are that the longitudinal components of k should not be too much smaller than the transverse momentum. Where the approximations and standard power-counting hold for the soft region, we deduce that

$$|k^- k^+| \gg k_T^2 \frac{m^2}{Q^2}. \quad (5.54)$$

We now ask when the conditions fail. If the failure is only of the conditions on the rapidity of k , that simply takes us to one of the collinear regions; this does not concern us here since we treat the collinear regions separately. However, a failure of (5.54) is problematic. When this condition fails, we have $|k^+ k^-| \ll k_T^2$. This puts k in a region called the Glauber region (Bodwin, Brodsky, and Lepage, 1981) in view of its importance in final-state interactions in high-energy scattering. The same region was also termed the ‘‘Coulomb region’’ in Collins and Sterman (1981).

In the case we are currently treating, the vertex function, we can perform a contour deformation on either or both of k^+ and k^- to get out of the Glauber region. Consider first the k^+ integral in the Glauber region. We can neglect k^+ compared with p_A^+ in the $p_A - k$ denominator; this is generally true when k is soft. We can also neglect k^+ in the gluon denominator, specifically because of the Glauber-region condition $|k^+ k^-| \ll k_T^2$. This leaves the denominator $(p_B + k)^2 - m^2 + i0 \simeq 2p_B^- k^+ - k_T^2 + p_B^2 - m^2 + i0$, and we can therefore deform k^+ into the upper half plane. Similarly we can deform k^- into the lower half plane.

The limits of the deformation on k^\pm are given by other poles, notably that of the gluon. The deformed contour no longer goes through the Glauber region. So on the deformed contour in the soft region, the standard power-counting and the Grammer-Yennie approximation are valid. However, the denominators in the Grammer-Yennie approximation give extra singularities at $k^+ = 0$ and $k^- = 0$, i.e., in the Glauber region close to the poles on the quark propagators. Thus the denominators must be equipped with $i0$ prescriptions that do not block the contour deformation:

$$(\text{coll. } A)^k N_{k\lambda} (\text{coll. } B)^\lambda \simeq (\text{coll. } A) \cdot k \frac{1}{k^- - i0} N^{-+} \frac{1}{k^+ + i0} k \cdot (\text{coll. } B). \quad (5.55)$$

In the previous paragraphs, there is a change of the kind of pole avoidance under discussion compared with the earlier part of this chapter. Initially, we viewed momenta relative to the large scale Q , and determined whether or not momentum components were forced go through regions where they are much smaller than Q . Now we are examining a soft momentum, of size $\lambda_S \ll Q$, and are determining whether or not its plus and/or minus components are forced to go through regions where they are much smaller than λ_S .

Although we derived it only for the one-loop graph, the contour deformation applies very generally to avoid the Glauber region in our process. Consider a general reduced graph (Fig. 5.29) for the vertex, and let k be a momentum flowing down on a soft line from the upper collinear graph B . We know that the flow of minus momentum in the B

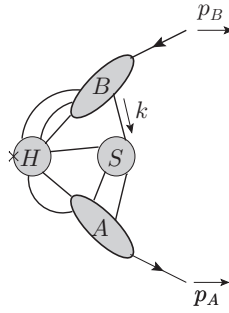


Fig. 5.29. Reduced graph for vertex.

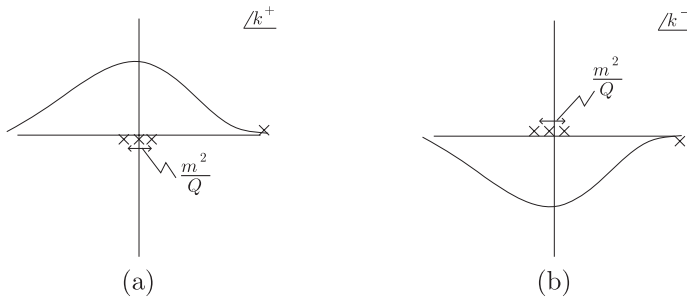


Fig. 5.30. Contour deformations out of Glauber region for (a) k^+ , (b) k^- . The crosses near the origin are final-state Glauber-region poles in collinear subgraphs. The crosses near the edges are other poles that limit the contour deformation.

subgraph is all towards the future, from the hard subgraph H to the final-state particle p_B . There must be a sequence of lines in B that gets to the vertex with line k from H by going forward with the flow of the minus component of momentum. We can choose to set up k as a loop momentum that goes along these lines, and completes its loop through H and A .

If k^+ is small enough for k to be in the Glauber region, then the only important dependence on k^+ is in B . Since k goes with the flow of collinear minus momentum, all the nearby poles are in the lower half plane, as in

$$\frac{1}{(k_B + k)^2 - m^2 + i0} \simeq \frac{1}{2k_B^- k^+ - D + i0}. \tag{5.56}$$

Here k_B is a generic collinear momentum on a line of subgraph B , and D does not depend on k^+ . Thus the same contour deformation into the upper half plane works as for the one-loop graph. A similar argument applies to a Glauber momentum attaching to the A subgraph.

This situation is illustrated in Fig. 5.30, and we characterize it by saying that all singularities in subgraphs A and B are in the final state; the lines in A and B all go out to the

future from the hard scattering. To see a direct relation to a space-time picture, we simply Fourier-transform (5.56) into coordinate space, with the soft-gluon approximation that only the k^+ dependence of the propagator is retained:

$$f(x) = \int \frac{d^4k}{(2\pi)^4} \frac{e^{-ik \cdot x}}{2k_B^- k^+ - D + i0} \simeq \frac{-i}{2k_B^-} \delta(x^+) \delta^{(2)}(\mathbf{x}_T) \theta(x^-) e^{-ix^- D/(2k_B^-)}. \quad (5.57)$$

When $x^- < 0$, we get zero, because the integrand decreases rapidly to zero in the upper half plane of k^+ , so that we can close the k^+ contour in the upper half plane. But when $x^- > 0$ we close the contour in the lower half plane and pick up the residue of the pole. More generally, for any function whose singularities in k^+ are only in the lower half plane, its Fourier transform is non-zero only for positive values of x^- . This is so general a property that the contour-deformation result applies beyond perturbation theory.

The delta functions in (5.57) show that, from the point of view of a soft gluon, the collinear subgraph is a line going to the future in a light-like direction from the hard scattering, so that the soft gluon does not resolve any internal structure of the collinear system.

5.5.11 Soft-quark regions, $R_{A'}$ and $R_{B'}$

The remaining PSSs for the one-loop vertex graph are $R_{A'}$ and $R_{B'}$, where one of the fermion lines is soft. Power-counting like that for the soft-gluon case, R_S , gives a suppression by at least one power of Q . Our general treatment, Sec. 5.8, will show that this happens because one end of a soft-quark line is at the hard subgraph instead of a collinear subgraph.

5.6 Which reactions have a pinch in the Glauber region?

For the vertex graph, the ability to deform out of the Glauber region is tied to the collinear lines all being final-state lines. We now ask for situations in which we cannot perform this deformation. This requires reactions in which both initial-state and final-state collinear lines are present. See Ch. 14 for some of the resulting complications. The reduced-diagram technique enables us to diagnose these cases very readily, and in fact we already have a supply of interesting examples.

Reactions for hadron production in e^+e^- annihilation via a single virtual photon will always have the hadrons in the final state. Hence these reactions are always safe from the Glauber region.

For DIS (Figs. 5.13 and 5.14) the jets are always outgoing, so contour deformation out of the Glauber region is possible for k^- . Target-collinear lines can be in both the initial and final state (Fig. 5.13(b)) so k^+ is trapped. But to avoid the Glauber region, it turns out to be sufficient that a deformation can be made on k^- (Collins, 1998b; Collins and Metz, 2004). This applies equally to variations on DIS, like deeply virtual Compton scattering and exclusive meson production in DIS.

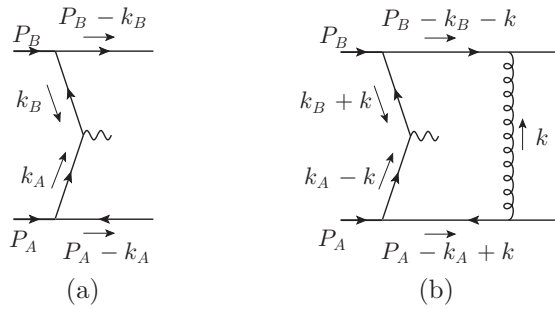


Fig. 5.31. (a) Simple Feynman graph for DY process. (b) The same with addition of a gluon exchanged between the spectator lines; the gluon’s momentum is trapped in the Glauber region.

5.6.1 Remnant-remnant interactions in Drell-Yan

The situation changes for the Drell-Yan (DY) process,⁵ since the initial state has two oppositely moving hadrons, and the final state contains the beam remnants (Fig. 5.17).

Physically, what happens can be seen in the microscopic view of a scattering reaction in Fig. 5.18. One parton out of each hadron collides at the short-distance hard interaction indicated by the star. The transverse separation of these two active partons is of order $1/Q$, corresponding to the scale of the hard collision. Inside the hadrons, partons are spread out over a transverse area proportional to r^2 , where $r \simeq 1$ fm is the size of a hadron. The transverse area is not changed under a boost. The probability that a pair of partons is within $1/Q$ of each other in the transverse direction is therefore proportional to $1/(Qr)^2$, which corresponds to a hard-scattering cross section decreasing with $1/Q^2$ at large Q .

But when the active partons collide, the remnants of the two hadrons overlap, and can therefore interact. Remnant-remnant interactions of small momentum transfer occur with high probability, since such hadronic interactions are strong. One direct manifestation is that the total hadron-hadron cross section is of order r^2 (Amsler *et al.*, 2008). Thus we know experimentally that interactions happen with high probability whenever the impact parameter of a pair of hadrons is less than about r . The strong remnant interactions involve momentum exchanges in the Glauber region.

5.6.2 Glauber pinch in momentum space

We now verify from an example that spectator-spectator interactions are trapped in the Glauber region for the Drell-Yan process, and that they give a leading power. In Fig. 5.31 are shown two graphs for the Drell-Yan amplitude when the beam particles are modeled by elementary particles. In both graphs, each beam particle splits into a quark-antiquark pair. A quark out of one beam annihilates with an antiquark out of the other to make a high-mass

⁵ And generally for hard processes in hadron-hadron collisions.

virtual photon. Graph (a) gives an example of pure parton-model physics, but graph (b) has a gluon exchanged between the beam remnants, and I will show that the gluon is trapped in the Glauber region.

The value of graph (a) is

$$-\bar{u}_B \Gamma_B \frac{-\not{k}_B + m}{k_B^2 - m^2 + i0} \gamma^\mu \frac{\not{k}_A + m}{k_A^2 - m^2 + i0} \Gamma_A v_A. \tag{5.58}$$

Here u_B and v_A are the Dirac wave functions for the final-state fermions. The matrices Γ_B and Γ_A give the coupling between the beam particles and quarks. We choose the kinematic region where the fermions are prototypically collinear, with transverse momenta of order m , as is appropriate for the parton model. The large components of k_B and k_A are determined by the virtual photon momentum (5.15), so that

$$k_A = (x_A P_A^+, 0, \mathbf{0}_T) + (O(m^2/Q), O(m^2/Q), O(m)), \tag{5.59}$$

$$k_B = (0, x_B P_B^-, \mathbf{0}_T) + (O(m^2/Q), O(m^2/Q), O(m)). \tag{5.60}$$

Graph (b) gives

$$\begin{aligned} & i g^2 \int \frac{d^4 k}{(2\pi)^4} \frac{1}{k^2 - m_g^2 + i0} \bar{u}_B \gamma^- \frac{\not{P}_B - \not{k}_B - \not{k} + m}{(P_B - k_B - k)^2 - m^2 + i0} \\ & \times \Gamma_B \frac{-\not{k}_B - \not{k} + m}{(k_B + k)^2 - m^2 + i0} \gamma^\mu \frac{\not{k}_A - \not{k} + m}{(k_A - k)^2 - m^2 + i0} \\ & \times \Gamma_A \frac{-\not{P}_A + \not{k}_A - \not{k} + m}{(P_A - k_A + k)^2 - m^2 + i0} \gamma^+ v_A, \end{aligned} \tag{5.61}$$

where the gluon couplings are replaced by their dominant minus and plus components. The gluon has transverse momentum of order the usual radial variable λ_S for the soft PSS, and the most characteristic value to model non-perturbative hadronic interactions is $\lambda_S \sim m$.

We first make approximations that are always valid when the gluon is soft, independently of whether it is in the Glauber subregion. So we neglect k^- with respect to k_B^- in the collinear-to- B denominators, and similarly for k^+ in the collinear-to- A denominators. Thus

$$\begin{aligned} (k_B + k)^2 - m^2 + i0 & \simeq 2(k^+ + k_B^+)k_B^- - (\mathbf{k}_T + \mathbf{k}_{BT})^2 - m^2 + i0 \\ & = 2k^+k_B^- + k_B^2 - m^2 - 2\mathbf{k}_T \cdot \mathbf{k}_{BT} - k_T^2 + i0 \\ & = 2k^+k_B^- + O(m^2, m\lambda_S, \lambda_S^2) + i0. \end{aligned} \tag{5.62}$$

This approximation needs the assumption that all components of k are much less than Q , but it needs no assumption on the relative sizes of the components.

If k were in the generic part of the soft region we could further approximate by noting that $k^+k_B^-$ would be of order $\lambda_S Q$, so that

$$(k_B + k)^2 - m^2 + i0 \simeq 2k^+k_B^- + k_B^2 - m^2 + i0. \quad (k \text{ not Glauber}) \tag{5.63}$$

But this further approximation fails in the Glauber region, $|k^+k^-| \ll k_T^2$.

The relevant part of the integral (5.61) now becomes

$$\int \frac{dk^+ dk^-}{(2\pi)^2} \frac{\text{numerator}}{2k^+k^- - k_T^2 - m_g^2 + i0} \times \frac{1}{[-2k^+(P_B^- - k_B^-) + \dots + i0][2k^+k_B^- + \dots + i0]} \times \frac{1}{[-2k^-k_A^+ + \dots + i0][2k^-(P_A^+ - k_A^+) + \dots + i0]}, \quad (5.64)$$

where the terms indicated by “...” are independent of k^+ and k^- , and are of order $m^2, m\lambda_S, \lambda_S^2$. In the Glauber region, $|k^+k^-| \ll |k_T|^2$, only the poles on the collinear lines are relevant. We see immediately that k^+ and k^- are trapped there, with $k^\pm = O(m^2, m\lambda_S, \lambda_S^2)/Q$, to be compared to $k_T = O(\lambda_S)$.

The dominant contribution is in fact where $\lambda_S = O(m)$. Smaller values are cut off by the gluon mass, while there are enough powers of k_T^2 in the denominators to suppress larger values, given our assumption about the collinear kinematics of k_A and k_B .

The asymmetric sizes, $k^\pm = O(m^2/Q)$ and $k_T = O(m)$, correspond to the momentum exchanged in small-angle elastic scattering. They are therefore natural values for spectator-spectator interactions. The sizes of k^\pm correspond to the small components of collinear momenta.

To obtain the power law in Q , we compute the size of the graph compared with the basic graph, Fig. 5.31(a). The extra Glauber gluon brings in the following powers:

- integration measure: m^6/Q^2 , from the sizes of k^\pm and k_T ;
- three denominators each of order $1/m^2$;
- a numerator of order Q^2 because the gluon is a vector particle.

This is independent of Q , with the numerator canceling the small range of k^\pm . If the space-time dimension is changed from $n = 4$, we still get the same power of Q . The basic graph, Fig. 5.31(a), has the power-counting of the parton model, which we use to define the leading power for the process. Therefore, there is an unsuppressed contribution from Glauber corrections. This result is unchanged if we make the collinear subgraphs arbitrarily complicated.

5.6.3 Generalized Landau-equation analysis for Glauber region

The actual integrals for Feynman graphs are in a high dimension. So, as in the elementary association between regions and massless PSSs, one can ask whether there is a possibility of an unforeseen exotic deformation in the high-dimensional complex space, and one can ask for a general characterization of Glauber regions. In a one-loop example, it was sufficient to visualize the relevant one-dimensional contour integrals. I now give an appropriate argument, generalized from the Libby-Sterman method.

In the first part of this chapter, we scaled all momentum components with Q . From this, we showed that integration momenta are trapped at small virtualities in the vicinity of exact

PSSs in the massless limit. The Landau method determined the locations of the PSSs quite generally.

To determine the existence or non-existence of a Glauber pinch, we generalize this strategy. We devise a scaling such that a trapping in a Glauber region corresponds to an exact pinch in a certain limit. Then we use a variation of the Landau analysis to locate the exact pinches systematically.

First I show that an exact Glauber pinch occurs when we replace the collinear denominators by just the terms of the form that are the non-dotted terms in (5.64). These terms are given by taking the asymptotics of large Q while holding the overall size of the soft momentum fixed at order λ_S , and treating the collinear scaling factor as λ_S . (Thus the transverse parts of collinear momenta are treated as order λ_S .) For this limit we also require that λ_S is of order m or bigger. Asymptotically, the propagator of the soft line remains unaltered, but the collinear denominators are simplified, so that they are just a factor of k^+ or k^- times a large component of the collinear momentum, e.g.,

$$\frac{1}{k^2 - m_g^2 + i0} \times \frac{1}{[-2k^+(P_B^- - k_B^-) + i0] [2k^+k_B^- + i0]} \times \frac{1}{[-2k^-k_A^+ + i0] [2k^-(P_A^+ - k_A^+) + i0]}. \quad (5.65)$$

The trapping of k^\pm at $k^\pm \ll \lambda_S$ has now become an exact pinch at $k^\pm = 0$. The on-shell condition for the collinear-to- B propagators is $k^+ = 0$, and for the collinear-to- A propagators is $k^- = 0$. In the chosen scaling limit, the on-shell conditions apply independently of \mathbf{k}_T , which represents a significant change from the standard Landau analysis. At the singularities, at $k^+ = 0$ and/or $k^- = 0$, the gluon denominator is non-zero, so the gluon line counts as part of a vertex of a reduced graph for this analysis: it is a hard subgraph relative to the collinear propagators.

To determine allowed directions of contour deformation, we need derivatives of the collinear propagators, as in (5.25). The derivatives of the collinear denominators are now exactly light-like directions. In space-time, these correspond to propagation along a light-like line, as in (5.57). For example, the collinear-to- B lines give

$$\frac{\partial D(P_B - k_B - k)}{\partial k^\mu} \longrightarrow \begin{pmatrix} -2(P_B^- - k_B^-) \\ 0 \\ \mathbf{0}_T \end{pmatrix}, \quad (5.66)$$

$$\frac{\partial D(k_B + k)}{\partial k^\mu} \longrightarrow \begin{pmatrix} 2k_B^- \\ 0 \\ \mathbf{0}_T \end{pmatrix}. \quad (5.67)$$

We have used column vectors for the derivatives, to distinguish them from the row vectors we use for normal contravariant momentum vectors. In the asymptotic limit these vectors are opposite in direction, so that when we apply a contour deformation, as in (5.24), the imaginary parts generated by the deformation are opposite; the deformation fails.

Applying this analysis in general shows that the general Glauber-pinch configuration is like having one or more extra hard scatterings (of the spectator collinear lines). The condition for a classical scattering applies, and the only change with respect to the standard hard-scattering case is the much lower momentum transfer.

5.7 Coordinates for a PSS

We now resume our general analysis. So far, we have used the Landau-equation/reduced-diagram method to locate PSSs; this led to a catalog of important momentum regions. We next formalize and systematize the variables we use for a general treatment, after giving a general characterization of the class of problems we address.

For each PSS R we will define “intrinsic coordinates”, which parameterize location on the PSS itself, and normal coordinates, which parameterize deviations off the PSS. The normal coordinates are required to be zero on the PSS. From the normal coordinates, we will define a radial coordinate λ_R , with the dimensions of mass, to give a notion of distance from the PSS. Then we will define what we term angular coordinates to parameterize surfaces of fixed λ_R surrounding the PSS.

This gives us a language, which lets us perform power-counting in Sec. 5.8, to determine which PSSs are leading. These results then support all the later work in this book.

For any of the reactions that we discuss, there is an intimidating multiplicity of regions, and this comes from a genuine complexity: there are infinitely many graphs, and high-order graphs have high-dimensional loop integrations, with a large number of leading regions. In QCD, unadorned low-order perturbative calculations are not adequate for estimating cross sections, except in very few cases, as in Ch. 4. So, to get a useful and productive analysis of the behavior of some amplitude or cross section, we need general methods that do not require detailed analysis of individual graphs.⁶

The general strategy is essentially a recursive divide-and-conquer. We discuss each leading region separately, and arrange to analyze it in terms of diagrammatic decompositions such as Fig. 5.17. By our choice of coordinates, the analysis of a general region can be visualized by a diagram that appeared in one of our examples, Fig. 5.28. At the end, it will (perhaps) be evident that there are structures here that go beyond the perturbatively based situations in which we derive them.

5.7.1 Relations between regions

The key elements of a general discussion are the geometrical and topological relations between different regions, as in (5.21) and in Fig. 5.28. We take a particular point on some PSS R for a graph, and examine a neighborhood, parameterized by a radial variable λ_R .

- Some propagators are off-shell at the PSS. For these, the effect of varying λ_R is suppressed by a power of λ_R/Q , and the denominators have a fixed order of magnitude.
- Denominators of the other propagators go to zero when λ_R and masses go to zero.

⁶ But motivations can be obtained by analyzing suitable low-order graphs.

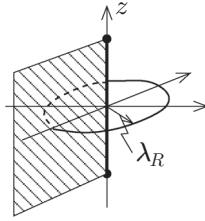


Fig. 5.32. Representation of line/surface of constant λ surrounding a PSS R at a particular value of the intrinsic coordinate(s), together with the relation to bigger and smaller PSSs. See the text for details.

- At a generic point around a surface of fixed λ_R , we perform elementary power-counting for the order of magnitude of the graph at R .
- But close to certain submanifolds of a fixed λ_R surface, some denominators get much smaller than the power-counting estimate. The location of these submanifolds will be obtained in Sec. 5.10 by iterating the Libby-Sterman analysis. With certain exceptions, each such submanifold corresponds to the intersection of the surface of fixed λ with the PSS for another region R' larger than the first one.

The general situation is illustrated in Fig. 5.32. The thick vertical line represents the PSS R , and there may be smaller PSSs, represented by the dots at the ends of R . There may be one or more larger PSSs, exemplified by the shaded plane at the left of the figure. Surrounding R , at a fixed value of the intrinsic coordinate(s), is a line of constant λ_R . The integration contour, and therefore Fig. 5.32, is deformed in the space of complex momenta to avoid non-pinch singularities.

In the figure the dimension of R is one, while the dimensions of the smaller and larger PSSs are zero and two. But in general, R may have any dimension from zero for a soft-gluon region in a one-loop vertex to a very high dimension in a multiloop graph, with appropriate ranges for the smaller and bigger PSSs.

- There are exceptions to the rule that, in the integration over angular variables, intersections with larger PSSs determine the locations where the integrand gets much smaller than the standard for R . These are typified by the Glauber region we met in Secs. 5.5.10 and 5.6. In processes without a Glauber pinch, we do not have to worry about the exceptions.
- After the intrinsic coordinates for R are integrated over, the integration includes smaller PSSs, and we need to mesh the analysis of R with the analysis of the smaller PSSs.
- Factorization theorems generalizing the parton model are obtained by expanding in powers of λ_R about a PSS, and then (typically) taking the leading power. The previous items will tell us how to modify this analysis to deal with multiple regions.

5.7.2 Formulation of problem

We denote by $G(p_1, \dots, p_n; q_1, \dots, q_m, \mu, a_s(\mu))$ the Green function, amplitude or cross section to be treated. It depends on external momenta $p_1, p_2, \dots; q_1, \dots$. We divide these

into two classes, to be defined below, distinguished by the letters p and q . This generalizes the usage in DIS, where p is the target momentum and q is the virtual photon momentum.

The asymptotic behavior to be treated is specified by a scalar variable Q that gets large. We work in a particular frame like the center-of-mass frame for the DY process, or the Breit frame for DIS. We call this the reference frame for the process. In this frame all the external momenta have some components of order Q . The p_j momenta have fixed masses, while the q_j momenta have invariant sizes of order Q^2 . [Here we mean $\Theta(Q^2)$ in the notation of App. A.17.] The q_j s are typically fixed vectors proportional to Q , or are obtained from such a vector by at most a finite, bounded boost from the reference frame. We also rule out the trivial but irrelevant case of giving a common large boost to a set of fixed momenta p_j . A Lorentz-invariant characterization is as follows.

1. Define scaled momenta by $\tilde{p}_i^\mu = p_i^\mu / Q$, $\tilde{q}_i^\mu = q_i^\mu / Q$.
2. We take Q large (i.e., much larger than particle masses) with each of the scaled external momenta smoothly approaching a fixed limit as $Q \rightarrow \infty$.
3. The limit of each \tilde{p}_i is a light-like vector, and the limit of each \tilde{q}_i is a non-light-like vector.
4. From the light-like limit vectors, we construct a set of unscaled light-like momenta $p_{A,\infty}$, $p_{B,\infty}$, etc., as in our examples, e.g., $p_{A,\infty} = Q \lim_{Q \rightarrow \infty} \tilde{p}_A$. Associated with each collinear subgraph is one such light-like momentum, which we will call the reference momentum for the subgraph. At the PSS, the momenta of the lines of the collinear subgraph are proportional to its reference momentum.
5. At least one of the Lorentz invariants $q_i \cdot q_j$, $q_i \cdot p_j$, and $p_i \cdot p_j$ increases like Q^2 as $Q \rightarrow \infty$; none increases more rapidly.

Since this is intended to be a universal characterization, the following caveats apply.

- Some of the limiting light-like vectors may be proportional to each other. This is the case, for example, for the momenta p and p' in the DVCS process. So we just pick one of these to be in the set of $p_{A,\infty}$, etc.
- Certain minor variations on the theme are also covered; for example:
 - In the Drell-Yan cross section, the transverse momentum may range from very small to order Q ; it may also be integrated over. The key point for the asymptotic analysis is that the invariants q^2 , $p_A \cdot q$, $p_B \cdot q$, and $p_A \cdot p_B$ are all of order Q^2 .
 - Some quark and hadron masses may be large, of order Q or bigger.
- There may be no need for the q_j momenta. This is the case for high-energy elastic scattering at wide angle, where the momenta of the external particles are sufficient to specify the process. The previously stated principles tell us to define $Q = \sqrt{s}$, up to some constant factor.
- We take G to be connected. A disconnected amplitude can always be discussed in terms of its connected components.

A more serious complication is when the invariants have a range of sizes. A typical and important case is DIS at small x , when $p \cdot q \propto Q^2/x \gg Q^2$. Another case would be

high-energy elastic scattering at small angle, where $|t| \ll s$. A complete discussion of such situations requires a generalization of our analysis.

5.7.3 Intrinsic and normal coordinates

We now show how to define intrinsic and normal coordinates for a PSS. These generalize our earlier examples.

For the collinear-to- A PSS of the vertex graph, we used $z = k^+ / p_A^+$ as the sole intrinsic coordinate, in (5.18), with k^- and k_T as the normal coordinates. The smallest PSSs, R_S , $R_{A'}$ and $R_{B'}$, were just points. Thus they had no intrinsic coordinates, while suitable normal coordinates were 4-momentum deviations from the PSS, e.g., k for R_S .

Naturally, the choice for these coordinates is non-unique. But certain general guidelines apply. Each coordinate system is particularly useful in a neighborhood of its own PSS. But it must apply to the whole of loop-momentum space, or at the very least to a large region of size of order Q including the PSS. The transformation from the local coordinates around the PSS to ordinary momentum variables must be analytic, certainly near the PSS and its smaller PSSs. The intrinsic coordinates extend uniquely beyond the boundaries of their PSS. Without this requirement, artificial coordinate singularities would complicate all our discussions.

Each line in a *reduced* diagram for a PSS in a massless theory has a momentum parallel to one of the light-like limit momenta, or is zero. For the collinear lines we choose intrinsic coordinates as fractional momenta, each with respect to the light-like limit momentum, e.g., $p_{A,\infty}$, of its collinear subgraph. The remaining intrinsic variables are the hard loop momenta. Now each PSS is a segment of a flat hyperplane in loop-momentum space. So with the definitions just given, the intrinsic coordinates of a PSS extend simply and naturally to the whole of the hyperplanes, beyond the boundaries of the regions where there is a pinch. Similarly we take the normal coordinates to be ordinary linear coordinates in momentum space. Thus there is a unique natural extension of the coordinates to the whole of loop-momentum space. (Our treatment of collinear regions for the vertex graph illustrated this.)

5.7.4 Radial coordinates

We obtain the power-counting for a PSS from the integral over a radial coordinate λ , for which we now present a suitable definition. We choose λ to have the dimensions of mass.

To make the definition, we split the normal coordinates into two sets. One set consists of soft loop momenta circulating through soft and possibly some collinear and hard subgraphs. The other set consists of collinear loop momenta each circulating through a particular collinear subgraph and possibly through hard subgraph(s).

We will write each individual normal component as a power of λ times a dimensionless angular variable and a possible Q -dependent normalizing factor, as in (5.29) and (5.49), with a chosen normalization condition on the angular variables.

General collinear momenta

We specify the scalings for a collinear momentum exactly as for a collinear region for the vertex graph, but we need to define a light-front coordinate system separately for each collinear subgraph.

Let k be a collinear momentum in a particular collinear subgraph, and let p_∞ be the light-like reference momentum for the subgraph. We define time and spatial parts of vectors in the reference frame (e.g., center-of-mass) of the process as a whole. Plus and minus coordinates relative to p_∞ are

$$k^\pm \stackrel{\text{def}}{=} \frac{1}{\sqrt{2}}(k^0 \pm \mathbf{n} \cdot \mathbf{k}). \tag{5.68}$$

Here \mathbf{n} is a unit vector for the spatial direction of p_∞ . Then the transverse momentum is

$$k_\perp \stackrel{\text{def}}{=} k - \frac{k^+}{\sqrt{2}}(1, \mathbf{n}) - \frac{k^-}{\sqrt{2}}(1, -\mathbf{n}), \tag{5.69}$$

where the representations of vectors are in normal time-space coordinates, in the reference frame.

Then the scalings of k are defined by exactly (5.29), with p_A^+ replaced by $p_\infty^+ \propto Q$; that is, a scaling with λ^2 for k^- and a scaling λ for k_\perp .

Note that a covariant specification of the plus and minus coordinates needs *two* 4-vectors. In effect, we have taken these as the light-like reference vector for the collinear subgraph, and the rest vector of the overall reference frame for the process.

Soft momenta

As in Sec. 5.5.9, we define the scaling for soft momenta by

$$k_S = \frac{\lambda^2}{Q} k_S. \tag{5.70}$$

Thus the power-counting of a soft momentum flowing through a collinear subgraph is the same as the smallest component of a collinear momentum, and the time scales of the soft and collinear lines are the same.

Normalization condition

A possible normalization condition on the angular variables is

$$\sum_{\text{collinear } k} (|\bar{k}^-| + |\bar{k}_\perp|^2) + \sum_{\text{soft } k} \sum_\mu |\bar{k}^\mu|, \tag{5.71}$$

which generalizes (5.31) and (5.46), with suitable homogeneity properties under rescaling of λ .

5.8 Power-counting

A basic issue in analyzing processes of the kind described in Sec. 5.7.2 is to understand the general size of the cross section or amplitude. The primary complication is that propagator

denominators vary widely in size in the integration over loop momenta. To handle this issue, we use the language of PSSs in the massless theory.

In this section, for each PSS R , we categorize by a power of Q the contribution from integration over a neighborhood of R . We will identify those PSSs that give the leading power for the processes we consider. For deriving factorization, we normally only retain the leading power, e.g., for DIS the power Q^0 , which corresponds to Bjorken scaling. The restriction to the leading power is important because PSSs with a non-leading power often have a much more complicated structure than those for the leading power.

In deriving the power laws, we will see that logarithmic enhancements arise from integrations between different nested regions. But logarithms do not affect the utility of dropping non-leading power terms.

The derivation involves estimates of the sizes of propagator denominators near a PSS. In later chapters a consequence will be the construction of an appropriate approximation for each leading PSS. These approximations enable the derivation of useful factorization theorems.

We will vary terminology between “PSS” and “region”. Precise formulations use PSSs in the massless theory. But we talk about a region, rather than the associated PSS, when we wish to emphasize, for example, that the associated power of Q concerns the contribution from a neighborhood of the PSS in the real theory.

The present formulation originates in the work of Sterman (1996), but with improvements, closely following the treatment of Collins, Frankfurt, and Strikman (1997). This treatment relies on general properties of dimensional analysis and of Lorentz transformations rather than on a detailed analysis of the numbers of loops, lines and vertices of graphs and subgraphs. Using such general properties, in particular the transformation of collinear subgraphs under large boosts, gives the results a validity beyond strict perturbation theory. Although much of the treatment concerns Feynman graphs, the collinear and soft factors should really be non-perturbative.

Much earlier work used an axial gauge (e.g., $A^0 = 0$, $A^3 = 0$, or $A^+ = 0$) or the Coulomb gauge. However, the unphysical singularities in the gluon propagator for such “physical gauges” prevent us from using contour deformation arguments. Thus we prefer to work in a covariant gauge – see the discussion of the Glauber region in Sec. 5.5.10, where unphysical singularities in physical gauges would have obstructed a contour deformation out of the Glauber region.

Therefore we normally use a covariant gauge, like the Feynman gauge. The price is that leading regions (e.g., Fig. 5.7(c) for DIS) have arbitrarily many extra gluons joining the collinear and hard subgraphs. But these gluons have a particular “scalar” polarization for which Ward identities apply to convert the sum over all possibilities to a factorized form.

5.8.1 Comments on power of Q and dimensions

A danger in formulating general results is that one misses nuances of particular cases. Consider the simplest general statement of the leading power of Q , that it corresponds

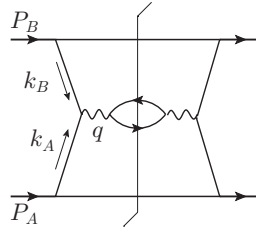


Fig. 5.33. Elementary contribution to Drell-Yan with single spectator.

to the dimension of the cross section or amplitude under consideration, as in (5.5). This rule is indeed correct for the DIS structure functions F_1 or F_2 , with their power Q^0 that corresponds to Bjorken scaling. But modifications are needed for certain other cases. For example, in Sec. 5.8.2 we will find that a different power is needed for the Drell-Yan cross section, in the case that the transverse momentum q_T is much less than Q .

The culprit is a delta function for transverse-momentum conservation. Essentially the derivations of power-counting are at their most straightforward when applied to ordinary functions, not to delta functions.

In general, a reliable strategy for dealing with such issues is to start by analyzing very simple graphs for the process under consideration, e.g., graphs such as Fig. 5.20 that gives the parton model for the Drell-Yan process, or, better still, just the lowest-order case, Fig. 5.33. A general region for the process can have more-complicated region subgraphs, and can have more lines joining the subgraphs. The changes *relative* to the simplest graph are robustly handled by our general derivation of the power-counting rules, in later sections. It is just the most basic situation that needs to be treated in a more process-specific fashion.

5.8.2 Power-counting for DY

To see these issues concretely, consider the fully differential cross section for the Drell-Yan process (5.14). This can be written as $d\sigma / d^4q d\Omega$, where q is the momentum of the lepton pair and $d\Omega$ is for the polar angles θ and ϕ that give the directions of the individual leptons. Since the lepton pair results from a single virtual photon, the angular distribution is a second-order polynomial in the sine and cosine of the polar angles; thus no special issues arise that depend on different regions of θ and ϕ . The cross section has an energy dimension of -6 , and the natural power law is Q^{-6} , where Q is the mass of the lepton pair $Q = \sqrt{q^2}$, assumed to be comparable with the center-of-mass energy.

This power law is in fact correct when the transverse momentum q_T of the lepton pair is comparable with Q . But I will now illustrate, by examining graphs of the form of Fig. 5.33, that when q_T is much smaller than Q , the power law must be changed to the much bigger value $1/(Q^4 q_T^2)$. This power is cut off by the effects of hadronic masses when q_T is of order a hadronic mass.

Let us write the graph as

$$\int d^4k_A d^4k_B B(k_B, P_B) A(k_A, P_A) H(k_A, k_B, q) \delta^{(4)}(q - k_A - k_B), \quad (5.72)$$

where A and B represent the upper and lower bubbles, while H represents the product of the amplitudes for the $q\bar{q} \rightarrow \mu^+\mu^-$ amplitude. Initially, we assume that the initial particles P_A and P_B are elementary, and for the purposes of understanding the power-counting it is sufficient to take the subgraphs A and B to be the simplest tree graphs, as in Fig. 5.33.

We must now investigate the following regions for Fig. 5.33, which can be distinguished by the values of the transverse components of the loop momenta:

- the purely hard region, where the whole graph forms the hard subgraph, so that both k_{AT} and k_{BT} are of order Q ;
- the single-collinear regions where only one transverse momentum is of order Q ; the other is power-counted as order $\lambda \ll Q$;
- the double-collinear region, where both k_{AT} and k_{BT} are much less than Q ; they are both counted as order λ .

In the purely hard region, dimensional analysis applies unambiguously to give the basic $1/Q^6$ power. There are delta functions in A and B to put the spectator particles on-shell. But these set the sizes of momentum components that are of order Q , and the dimensional analysis argument still works. In this region of loop momenta, the $1/Q^6$ power law applies independently of the value of the external transverse momentum q_T . The hadronic final state contains two jets of high transverse momentum, corresponding to the remnant partons, which have large transverse momentum.

Next, consider a single-collinear region; for definiteness let us choose k_A to be collinear to P_A , so that k_{AT} is of order λ . The other transverse momentum k_{BT} is large and must therefore flow out into the virtual photon. Hence this region only exists when the lepton pair has transverse momentum of order Q . This large transverse momentum is approximately balanced by a final-state jet formed by a remnant parton on the B side.

We can think of the collinear subgraph as having an approximate rest frame in which all components of its momenta are of order λ . Given that parton A is a quark, the collinear subgraph has dimension -3 ; the measure of the k_A integral has dimension $+4$, for a total dimension of $+1$. This corresponds to a power λ , instead of a power Q which we would obtain for the same subgraph in the purely hard region. But the subgraph is boosted from its rest frame. Each of the lines connecting it to the hard subgraph has spin- $\frac{1}{2}$, so that largest components of the spinors on each line gain a factor of $(Q/\lambda)^{1/2}$ from the boost, for a total of Q/λ . Thus the complete power law is $(\lambda/Q)^0$ relative to the purely hard case; that is, the overall power remains unchanged. Thus we still get the overall power Q^{-6} for a single-collinear region, but this region only exists for the large- q_T region.

It is worth noting that although the detailed argument depends on the spin of the quark, the power law does not. If we were to use a model with a scalar quark, then there would be no Q/λ enhancement from the boost, but the collinear subgraph, complete with its integral,

has dimension 0. So the overall power is unchanged. The same argument applies to gluons with transverse polarization. But a virtual gluon can also have a polarization in the direction of the large momentum, and boosting each of two gluons gives an enhancement by a factor $(Q/\lambda)^2$. But a Ward-identity argument will show that this part cancels after a sum over all possible hard subgraphs: see Ch. 11 for the simplest such derivation.

Finally, we examine the double-collinear region. The virtual photon has transverse momentum $\mathbf{k}_{AT} + \mathbf{k}_{BT}$, which is of order λ . The separate collinear subgraphs give an unchanged power of Q just as in the single-collinear region. However, in the delta function for transverse momentum conservation, $\delta^{(2)}(q_T - k_{AT} - k_{BT})$, all the momenta are of order λ . So the delta function power counts as $1/\lambda^2$ instead of $1/Q^2$. As previously announced, the result is an enhanced overall power of $1/(Q^4 q_T^2)$ instead of $1/Q^6$.

The phenomenological result is a strong enhancement at small q_T , as we will see in the data in Fig. 14.13. Evolution effects, to be treated in Chs. 13 and 14, will strongly modify the actual power law, so the power law just derived has exact applicability only for individual graphs. Of course the decrease is cut off at small enough λ that mass effects need to be taken into account.

We made an initial assumption, for simplicity, that the initial-state particles are elementary. But the dimensional-analysis argument applies to the collinear subgraphs even when the initial particles are composite. So we get the same power laws when the initial-state particles are normal hadrons, which entails the use of bound-state wave functions.

It is also useful to examine the cross section integrated over the transverse momentum q_T of the pair and also over the angle of the leptons, to give $d\sigma / dQ^2 dy$, where y is the rapidity of the lepton pair relative to the center-of-mass. In the small- q_T region, a factor λ^2 arises from the integration measure d^2q_T , which compensates the $1/\lambda^2$ factor in the differential cross section. Hence the integrated cross section power counts as Q^{-4} in all regions. Naturally there is a logarithmic enhancement from the integral to small transverse momentum, which leaves the power law itself unchanged.

We can summarize the source of the enhancement in the differential cross section at small q_T as being in the creation of virtual photon from two oppositely moving collinear partons, without production of extra jets. Technically the enhancement is associated with the transverse-momentum delta function in this situation, so that the collinear transverse-momentum integrals are linked. In regions with production of jets of high transverse momentum, as in Fig. 5.19, there is no enhancement. We therefore see a simplification of the leading regions relative to the case that q_T is of order Q . In compensation, the linking of the collinear transverse-momentum integrals introduces some very interesting extra features in the derivation and formulation of factorization, as we will see in Chs. 13 and 14.

5.8.3 Powers of Q and λ

We consider a generic point in the intrinsic variable(s) z , and examine the integral over the radial variable λ . There is an angular integral, represented by the ellipse in Fig. 5.32. Over

most of the angular integration, the sizes of the denominators (with masses neglected for now) obey the standard power-counting, Sec. 5.5.8:

$$\begin{aligned} \text{Hard:} & \quad Q^2, \\ \text{Collinear:} & \quad \lambda^2, \\ \text{Soft:} & \quad \lambda^4/Q^2 = \lambda_S^2. \end{aligned} \tag{5.73}$$

These sizes are not exceeded. Much smaller values may be obtained, but only close to certain submanifolds of the intrinsic variables or of the angular integration. These are where z gets close to the PSS for a smaller region than or where the angular variables get close to a larger region: Sec. 5.10.

Our basic strategy is to use dimensional analysis to convert these estimates for single lines to estimates for the whole hard, collinear and soft subgraphs. This is supplemented by factors implementing boosts of collinear subgraphs from their rest frame: these produce enhancements that increase with the spin of the lines connecting the collinear to hard and soft subgraphs.

For small λ all the denominators participating in the PSS R get small. For large $\lambda \sim Q$, they all become hard, i.e., they all have virtualities of order Q^2 . (Of course, this holds except for neighborhoods of PSSs R' that are bigger than R . In neighborhoods of these, some denominators remain small. But this happens only in a small part of the angular integration.)

To obtain the power of Q for a region, we start from an estimate of the λ -dependent part of the integral in the form

$$Q^{p_1} \int_0^{O(Q)} \frac{d\lambda}{\lambda} \lambda^{p_2}, \tag{5.74}$$

or some variation thereof, with the exponents p_1 and p_2 to be determined. At small λ , we should cut off the integral by the effects of masses, and at large λ we get to a purely hard region when $\lambda \sim Q$. We distinguish three different cases:

- The power of λ is zero: $p_2 = 0$. Then the integral is logarithmic and each order of magnitude in λ contributes equally. The resulting Q dependence is Q^{p_1} modified by logarithms, a very typical situation in QCD.
- The power of λ is negative. Then the integral would have a power-law divergence at $\lambda = 0$ were it not for mass effects. The physical result is therefore dominated by small λ , and we must examine the cutoff provided by masses. If the dominant cutoff is on collinear lines, then it is at $\lambda \sim m$, and the power law is still Q^{p_1} . If the dominant cutoff is on soft lines, then the cutoff on λ is \sqrt{mQ} , and the power of Q is $Q^{p_1+p_2/2}$.
- The power of λ is positive. Then the integral is dominated by its upper end, $\lambda \sim Q$, i.e., by a hard region rather than R . The power of Q for this hard region is $Q^{p_1+p_2}$. The contribution of the region R for a particular size of λ is of order $Q^{p_1} \lambda^{p_2}$, which is a power of Q less than the contribution of the hard region. Thus the region R itself is non-leading.

5.8.4 Overall form of power law

We now derive the power law for a general PSS R in the form

$$Q^p \left(\frac{\lambda}{Q}\right)^{\alpha(R)} \left(\frac{\lambda_S}{Q}\right)^{\beta(R)} \left(\frac{m}{Q}\right)^{\text{s.r.}(H)} \left(\frac{m}{\lambda}\right)^{\text{s.r.}(C)} \left(\frac{m}{\lambda_S}\right)^{\text{s.r.}(S)}. \quad (5.75)$$

The first factor is the characteristic power of Q for the process, e.g., the dimensional-analysis power for the Sudakov form factor or for DIS. As such, it is independent of the particular PSS R . The exponents in the second and third factors indicate how the power is modified by collinear and soft subgraphs. We will obtain formulae for the exponents in terms of the numbers of external lines of the various subgraphs defining the process and the regions.

The last three factors arise if there are super-renormalizable couplings in the theory. Although super-renormalizable couplings do not exist in QCD, it is useful to work with models with extra couplings. First, they allow us to see the result for a general QFT. Second, they do arise when we dimensionally regulate QCD. Finally, they help to give insight into the physical phenomena associated with the power-counting theorems. Furthermore, some equivalents of super-renormalizable couplings occur when external particles are bound states and collinear subgraphs contain their wave functions.

The above power law is intended to apply when we integrate over λ of some order of magnitude. Similarly, we assume that we have integrated over a range of the intrinsic variables that is of order their typical size, all the while staying away from smaller PSSs. Notice that, to let us easily read off the different effects of masses in the collinear and soft subgraphs, we wrote some factors in terms of λ and some in terms of the soft scaling variable $\lambda_S = \lambda^2/Q$. Factors involving λ_S are associated with the soft subgraph.

5.8.5 Basic power Q^p

Subject to the caveat in Sec. 5.8.1, the first factor Q^p in (5.75) is the dimensional analysis power for the amplitude or cross section under discussion. For a connected amplitude, dimensional analysis gives

$$p = 4 - \#(\text{ext. lines}), \quad (5.76)$$

where $\#(\text{ext. lines})$ is the number of external particles and external hard currents. In this estimate are included Dirac wave functions for external spin- $\frac{1}{2}$ fermions, which grow with energy like $Q^{1/2}$; the exponent is independent of the types of the external particles.

For example, for the current-quark-antiquark vertex of Fig. 5.1, we have three external lines, and therefore the power is Q^1 . In the case of a scalar quark, at lowest order the power is from the factor of momentum at the photon-quark-quark vertex. In the case of an ordinary Dirac quark, the vertex is a Q -independent Dirac matrix γ^μ ; the two external Dirac wave functions give the overall power Q^1 .

Another example is the DIS structure tensor $W^{\mu\nu}$, for which there are four external lines. This gives Q^0 , i.e., Bjorken scaling.

5.8.6 Formulae for the other exponents

I first state the formulae for the exponents $\alpha(R)$ and $\beta(R)$:

$$\alpha(R) = \#(CH) - \#(\text{scalar pol. glue } CH) - \#(\text{ext. lines}), \quad (5.77)$$

$$\beta(R) = \#(0 \text{ or } 1, SH) + \frac{3}{2}\#(\frac{1}{2}, SH) + \frac{1}{2}\#(0 \text{ or } \frac{1}{2}, SC), \quad (5.78)$$

and explain the meanings of the terms on the r.h.s.; these give the exponents in terms of the numbers of external lines of the different subgraphs for the PSS. Then I will state the formulae for the remaining exponents. In later sections I will derive the formulae.

In (5.77), $\#(CH)$ is the number of lines joining the collinear and hard subgraphs. When $\alpha(R)$ is used in (5.75) there is therefore a power suppression as the number of collinear lines joining the subgraphs is increased. We will see in Sec. 5.8.8 that, in the polarization sum for a gluon connecting a collinear to the hard subgraph, there is no power suppression when gluon has what we call scalar polarization. The second term on the right, $\#(\text{scalar pol. glue } CH)$, provides the necessary compensation to the first term. Finally $\#(\text{ext. lines})$ is the number of external particles of collinear subgraphs (e.g., a total of two for the two collinear subgraphs in a PSS for the Sudakov form factor).

The power $\beta(R)$ in (5.78) depends on the numbers of lines connecting the soft subgraph to the other subgraphs. The value depends on the spin of the lines, so we write, for example, $\#(0 \text{ or } \frac{1}{2}, SC)$ for the number of lines of spin 0 or $\frac{1}{2}$ connecting the soft to collinear subgraphs, and similarly for the other terms.

Notice that the formula for $\beta(R)$ implies that there is generally a suppression by a power of Q whenever lines join the soft to the collinear or hard subgraphs, the suppression increasing with the number of lines. But there is an exception, that there is no penalty for gluons joining soft to collinear subgraphs. Thus $\beta(R)$ is zero when the connections of the soft subgraph consist only of gluons to the collinear subgraphs. In all other cases $\beta(R) > 0$.

Finally, the other exponents in (5.75), $\text{s.r.}(H)$, $\text{s.r.}(C)$, and $\text{s.r.}(S)$, are the dimensions of the super-renormalizable couplings in the hard, collinear and soft subgraphs. In the corresponding factors, we use m to denote a mass scale for the typical size for these couplings.

5.8.7 Exponent for hard subgraph

Let the hard subgraph H have N_F external fermionic (Dirac) lines and N_B external boson lines. In normal QCD processes, this means that N_F is the number of quark plus antiquark external lines, while N_B is the number of external gluon lines, plus the number of external photon, W , Z , and Higgs lines. We always take the hard part to be one-particle irreducible in its external lines, so the dimension of H is $d_H = 4 - \frac{3}{2}N_F - N_B$. In the usual case that all the couplings are dimensionless, the power associated with the hard subgraph is just the usual UV power from dimensional counting with all momenta of order Q :

$$Q^{d_H} = Q^{4 - \frac{3}{2}N_F - N_B}. \quad (5.79)$$

The use of dimensional analysis shows that this power depends only on the external lines of the subgraph, not on the internal details. We will combine the above exponent with the results for collinear and soft subgraphs to give (5.75), (5.77), and (5.78).

If there are super-renormalizable couplings with combined mass-dimension D , they count as m^D instead of Q^D . This gives a correction factor relative to (5.79) of $(m/Q)^D$, i.e., the fourth factor in (5.75).

5.8.8 Exponents for collinear subgraph

Rest frame

The region may have one or more collinear subgraphs C , as in Figs. 5.7 and 5.16. For each collinear subgraph, we express the momenta of its lines in the light-front coordinates defined in (5.68) and (5.69). Our definition of the radial variable λ in Sec. 5.7.4 gives exactly the same power-counting as in the one-loop example in Sec. 5.5.2, so that both the integration measure for a generic collinear momentum k and denominators for collinear propagators count according to their dimensions, λ^4 and λ^2 respectively. In a collinear subgraph we include any collinear loop momenta that circulate through the hard subgraph.

In the collinear subgraphs, we also include the wave functions for external particles of the relevant collinearity class, and numerator factors. Their effect is assessed by boosting from (an approximate) rest frame.

Now in the *rest frame* of the collinear momenta, the power of λ is just given by its dimension: $\lambda^{\dim \text{ of subgraph}}$, apart from super-renormalizable couplings. The dimension of a connected collinear subgraph, including external Dirac wave functions, is

$$\#(C \text{ to } H) + \frac{1}{2}\#(\frac{1}{2}: C \text{ to } H) - \#(S \text{ to } C) - \frac{1}{2}\#(\frac{1}{2}: S \text{ to } C) - \#(C \text{ to ext.}), \quad (5.80)$$

with a notation like that in (5.77), and with $\#(C \text{ to ext.})$ representing the number of external lines connecting to the collinear subgraph. The different signs of the terms in (5.80) arises from the differences between amputated and unamputated lines at the edge of the subgraph, and from the loop integrals coupling the graph to the hard subgraph. If there are super-renormalizable couplings, they give a correction factor which is the fifth factor in (5.75), similarly to the case of the hard subgraph.

We sum (5.80) over all the connected collinear subgraphs, and obtain the same formula, with the terms like $\#(C \text{ to } H)$ now denoting the number of lines connecting all collinear subgraphs to the hard subgraph.

Boost of collinear subgraph

Next we boost each collinear subgraph to the overall center-of-mass frame. The result depends on the spins of the lines connecting the subgraph to the hard and soft subgraphs. For a field of spin- s , standard properties of representations of the Lorentz group show that its biggest component increases under the boost like $(Q/\lambda)^s$. For a Dirac field we have a power $(Q/\lambda)^{1/2}$, while for a gluon⁷ we have Q/λ . For a whole collinear subgraph, we need

⁷ Any result for a gluon applies also to any other spin-1 field, e.g., for the photon.

the product of one such power for each line joining it to the hard subgraph, and for each line joining it to the soft subgraph. (We have included external Dirac wave functions in the collinear subgraph(s), so they do not need to be allowed for separately.) Combining all the powers so far gives (5.75) except for soft-subgraph associated factors:

$$\text{Result in (5.75)} \times \lambda_S^{-\#(S) - \frac{1}{2}\#(\frac{1}{2}:S)}. \tag{5.81}$$

With one exception, the exponents, p , $\alpha(R)$, and $\beta(R)$ in the referenced formula (5.75) are given by (5.76)–(5.78), while $\#(S)$ is the number of all external lines of the soft subgraph, and $\#(\frac{1}{2} : S)$ is its number of spin- $\frac{1}{2}$ external lines [which also count in $\#(S)$]. We wrote the second factor in (5.81) in terms of $\lambda_S = \lambda^2/Q$, since that is the natural variable for the soft factor.

The exception about (5.81) concerns the gluons, where the derivation so far gives

$$\text{Preliminary: } \alpha(R) = \#(CH) - \#(\text{spin } 1: CH) - \#(\text{ext. lines}). \tag{5.82}$$

This is the exponent of λ/Q , so it implies that we have a penalty for every extra line joining the collinear and hard subgraphs, except for the gluons. The non-suppression of gluons arises from the plus component of the gluon polarization (in the direction of the collinear group it belongs to), because of the corresponding boost factor Q/λ .

But we will also use the transverse components, which do not undergo this boost. We now examine how to separate the contributions.

Collinear gluon polarization

We have already seen this phenomenon in examples. So let us examine a general decomposition of a connection of a gluon of momentum k from a collinear subgraph C to the hard subgraph H . We have a factor $C(k) \cdot H(k)$, where there is a contraction of the Lorentz index at the H end of the gluon. The gluon is collinear, so we define the collinear factor C to include the gluon’s propagator. We decompose $C \cdot H$ with respect to the light-front components for C :

$$C \cdot H = C^+ H^- + C^- H^+ - C_T \cdot H_T. \tag{5.83}$$

After the boost from the rest frame for the collinear subgraph, the largest component of C^μ is the C^+ component, which increases like Q/λ . Next is the transverse component C_T , which is boost invariant, and finally C^- , which decreases like λ/Q .

The largest term is therefore $C^+ H^-$, and this gives the power derived above, in (5.81) and (5.82). So we define a Grammer-Yennie decomposition:

$$H \cdot C = H \cdot k \frac{C^+}{k^+} + H_\mu \left(C^\mu - k^\mu \frac{C^+}{k^+} \right). \tag{5.84}$$

The highest power Q/λ for C^μ is in the first term alone, which we call the scalar polarization term, since it has a polarization vector proportional to the momentum of the gluon. It is of a form suitable for applying a Ward identity. The second term, a transverse polarization term, has the highest power removed: the quantity in parentheses is exactly zero when $\mu = +$. Therefore this term power counts as 1 instead of Q/λ .

We now apply this decomposition to every gluon joining the collinear subgraphs and H . Each gluon line gives a scalar polarization term and a transverse polarization term. This converts the exponent $\alpha(R)$ from the one in (5.82) to the one in (5.77).

The importance of this operation is as follows. We start with a case like the parton model for DIS where the hard scattering is induced by fermion lines, and to get a leading power, we use the minimum possible number of such lines, which is two for the structure function in DIS. Replacing the fermions by scalar polarized gluons increases the power of Q to Q^2 , giving a super-leading contribution. The super-leading contribution in fact cancels, as shown by the use of Ward identities (Labastida and Sterman, 1985). The remaining term is leading, and involves transversely polarized gluons.

Similar decompositions can be applied on fermion lines, but we will not need them here, because we will not have the same cancellation of the highest power.

5.8.9 Derivation of exponent for soft subgraph

We now bring in the soft subgraph S . All its external lines attach to the collinear and hard subgraphs. We include in S the integrals over loop momenta that circulate from S through the hard and collinear subgraphs, since these loop momenta are necessarily soft. The soft subgraph S may have one or more connected components.

A complication we have already noticed is that of choosing an appropriate scaling of the momenta. We let λ_S be the scaling factor for all the components of soft momenta. We have seen that to match the time scales of soft and collinear graphs, we need to take $\lambda_S = \lambda^2/Q$, where λ is the overall radial variable for the region under discussion. This contrasts with the treatment in Sterman (1996) where λ_S and λ were taken to be the same.

Without super-renormalizable couplings, our usual dimensional analysis argument applies in terms of λ_S to give a power

$$\lambda_S^{\#(S) + \frac{1}{2}\#(\frac{1}{2}:S)}, \quad (5.85)$$

where the exponent is the dimension of the soft subgraph, including its loop integrals to the collinear and hard subgraph. This power applies independently of the number of connected components of the soft subgraph. This power evidently cancels the second factor in (5.81), so the final power law is (5.75), with the exponents defined in (5.76), (5.77), and (5.78). If there are super-renormalizable couplings, they give the last factor in (5.75), by the same reasoning as for the other subgraphs.

5.8.10 Other scalings

The derivation of the power law assumed what we can call the canonical scaling of momenta for a region R – (5.29), (5.49), which led to (5.73) for the denominators. Could other cases matter? We have cataloged all pinch-singular surfaces of massless graphs for our process. The scalings parameterize a neighborhood of each region by a radial variable. To the extent that the estimates of the denominators in (5.73) are correct, our derivations are correct.

Where the denominators are much smaller than the estimates, our derivation is incomplete. We will see in detail later that these situations occur in three ways. One is around an intersection of a surface of constant λ with the PSS for a bigger region than R , as in Fig. 5.32. The second is where the intrinsic variables of R approach a smaller PSS. The final possibility is where there is a trap of the integration region in a Glauber-type region.

We will show that the power laws remain correct in the first two cases, but if there is logarithmic behavior in λ , i.e., a power λ^0 , then logarithmic enhancements in the Q dependence occur relative to the basic power. This is quite common.

For many processes of interest, the Glauber region does not contribute or cancels after a sum over allowed final-state cuts.

One complication arises when some particle masses are actually zero, and we have an actual infra-red or collinear divergence at $\lambda = 0$. In a theory of confined quarks and gluons these divergences are not genuinely physical, but they do appear in Feynman graphs. They are handled by a sufficiently careful treatment of the soft region as we have defined it.

5.8.11 Power of Q

From (5.75), we derive the power of Q associated with a region after integration over λ . An important case is that all the exponents $\alpha(R), \dots, s.r.(S)$ are zero, which corresponds to leading regions for processes like DIS and Drell-Yan. Then we simply get Q^p , which is the power corresponding to the dimension of the amplitude or cross section under consideration. There is no λ dependence in (5.75), so the integral (5.74) gives a logarithm of Q divided by a mass scale. When we discuss nested regions, in Sec. 5.10, we will find an extra logarithm for every level of nesting where power-counting gives a logarithmic radial integral. The actual result is then

$$\text{Standard leading power: } Q^p \times \text{logarithms.} \quad (5.86)$$

When one or more of the exponents is non-zero, the precise power of Q will depend on how masses cut off the integral at small λ . If there is no soft subgraph, then the cutoff is dominated by masses on collinear lines, so that the power of Q is determined by setting $\lambda \sim m$ and we get

$$\text{Coll. cutoff: } Q^{p-\alpha(R)-s.r.(H)} m^{\alpha(R)+s.r.(H)} \times \text{logarithms.} \quad (5.87)$$

If there is a soft subgraph, then the cutoff is at $\lambda_S \sim m$, i.e., $\lambda \sim \sqrt{mQ}$, and we get

$$\begin{aligned} \text{Soft cutoff: } & Q^{p-\frac{1}{2}\alpha(R)-\beta(R)-s.r.(H)-\frac{1}{2}s.r.(C)} \\ & \times m^{\frac{1}{2}\alpha(R)+\beta(R)+s.r.(H)+\frac{1}{2}s.r.(C)} \times \text{logarithms.} \end{aligned} \quad (5.88)$$

If there are both collinear and soft loops, the cutoffs can be different on the collinear and soft loops. This will result in an important contribution where the \bar{k} variables [see (5.29)] are particularly small on collinear lines. This will refer to a small part of the angular integral. In our discussion of nested regions, we will assign this part to another region.

5.9 Catalog of leading regions

We now obtain general rules for determining the leading regions for a process.

5.9.1 General principles

The general power law was given in (5.75). Rather than presenting a power of Q alone, we have included powers of λ and λ_S . Thus we can read off the effects of masses that cut off the integrals at their lower ends.

For each process there is a minimum number of collinear lines entering the hard scattering if the process is to occur kinematically. For example, this is one on each side of the final-state cut in DIS, and two on each side of the final-state cut for Drell-Yan. In all these cases this is the same as the number of external hadrons for the process as a whole. With this minimum number of lines, we get $\alpha(R) = 0$. This is provided that we exclude gluons of scalar polarization in the minimally connected graphs; as will be proved later, we get zero after summing over graphs when all the lines joining a collinear subgraph to the hard scattering are zero.

Thus with the minimal number of connections between the collinear and hard subgraphs, the power of Q is the same as the pure UV power, $Q^p = Q^{4-\#(\text{ext. lines})}$, which we define to be the leading power for the process, e.g., Q^0 for DIS.

After this we read off from (5.75)–(5.78) that we get a power suppression, when we do any of the following:

- attach extra collinear lines to the hard scattering, except for scalar polarized gluons;
- attach any soft lines to the hard scattering;
- attach the soft subgraph to the collinear subgraphs by anything but gluons.

But there is no penalty for extra scalar-polarized collinear gluons attaching to the hard scattering, and there is no penalty for soft subgraphs that attach to collinear subgraphs by gluon lines only.

As to super-renormalizable couplings, they always give a penalty in the hard scattering. But in the collinear and soft subgraphs, there is no penalty as long as the momenta are at the lower end of their range, near the mass cutoff. Note that in the limit of zero mass, super-renormalizable couplings convert otherwise logarithmic IR singularities to power-law singularities.

It is worth observing that our rules give no penalty for having quark loops *inside* the soft subgraph. This is a fact that is sometimes forgotten, because in the corresponding IR-divergence problem in QED, no loops of massive fermions need to be considered.

One complication that sometimes arises is that when one actually does a particular calculation, the coefficient of the leading power might be zero. Typically this arises because of some symmetry. A simple example is the polarization dependence of DIS. The power-counting argument permits a Q^0 behavior in $W^{\mu\nu}$ for the dependence on both longitudinal and transverse polarization. In fact only longitudinal polarization gives this behavior, in the structure function g_1 – see (2.20). But for transverse polarization, there is a

power suppression – see Sec. 6.1.4 for the parton-model case – which results from the chiral symmetry of QCD and QED perturbation theory for hard scattering.

5.9.2 Prescription for leading regions

From the results just derived, the leading regions in the examples earlier in this chapter are indeed those stated: e.g., Fig. 5.5 for the quark-quark-current vertex, Fig. 5.7(c) for DIS and DVCS. The general principles are:

1. The soft subgraph connects only to collinear subgraphs and only by gluons.
2. The collinear subgraph(s) each connect to the hard subgraph(s) by the minimum number of lines consistent with the desired process or reaction occurring at all.
3. In addition, arbitrarily many gluons of scalar polarization may connect a collinear subgraph to a hard subgraph.

Thus in DIS, two quarks, one on each side of the final-state cut, can join the target-collinear subgraph to the hard subgraph. This exactly corresponds to the idea that motivated the parton model. But the rules just stated show that it is possible to replace the quark lines by transversely polarized gluon lines. This corresponds to a short-distance scattering off a gluon constituent in the target, compatible with the basic short-distance scattering idea. However, the minimal hard scattering is the reaction $\gamma^* + g \rightarrow q\bar{q}$, for which the amplitude is one order higher in QCD perturbation theory than for scattering off a quark.

5.9.3 Possibility of multiple hard scatterings

A particularly non-trivial example is elastic scattering of protons at wide angle. The reaction is $P_1 + P_2 \rightarrow p_3 + p_4$. The incoming protons are in opposite directions, and the outgoing protons are in very different (and again opposite) directions. Thus there are four collinear directions, two in the initial state and two in the final state.

If we restrict our attention to reduced graphs with collinear and hard subgraphs, then one possibility is a single hard subgraph, as in Fig. 5.34(a). Now a single quark has baryon number $\frac{1}{3}$, so a minimum of three quarks out of the collinear subgraph for each proton must attach to the hard scattering; otherwise, for example, remnants of the incoming protons would be left in the final state, approximately parallel to the incoming hadrons.

The connected hard scattering subgraph has 12 quark lines, which, from (5.76), corresponds to a power $1/Q^8$ in the amplitude, or equivalently $1/s^4$. Converting to a cross section gives $d\sigma/dt \propto 1/s^{10}$, as first found by Brodsky and Farrar (1973).

But it is also possible to have three separate quark-quark hard scatterings: Fig. 5.34(b). As shown by Landshoff (1974), this results in less of a suppression, giving $d\sigma/dt \propto 1/s^8$. The derivation needs a generalization of the results earlier in this section, both because the hard scattering is disconnected, and because of the associated momentum-conservation delta functions.

There are also a number of other possibilities that need to be examined, including a single quark-quark hard scattering, with the other quarks being soft. Soft quarks normally give

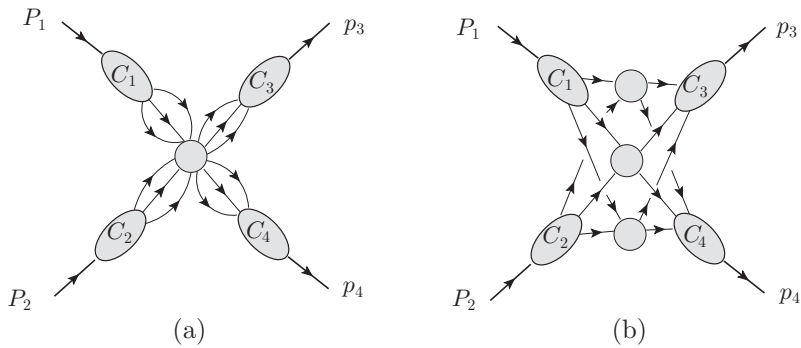


Fig. 5.34. Possible reduced graphs for wide-angle elastic proton-proton scattering: (a) with connected hard subgraph, (b) with three separate hard subgraphs. The elliptical blobs labeled C_j are collinear, and the unlabeled circular blobs are hard.

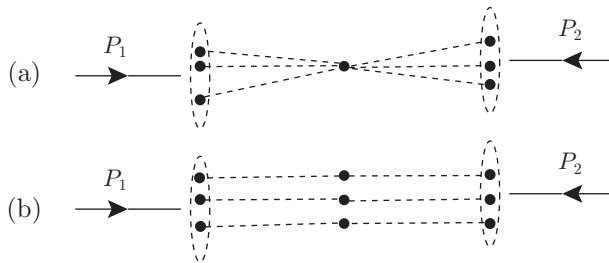


Fig. 5.35. Side views of the spatial structure corresponding to the reduced graphs of Fig. 5.34.

a power-suppression, but here this is compensated by not needing so many lines entering the hard-scattering subgraph(s). A correct analysis also needs to account for the Sudakov suppression of the hard scattering in the Landshoff graph, because each subgraph involves isolated color.

The difference between the mechanisms can be understood in space-time. With a single hard scattering, all the quarks in each proton must come down to within a transverse distance $1/Q$ of each other: Fig. 5.35(a). This gives a strongly power-suppressed probability, since the normal transverse separation of the quarks is of the order of 1 fm.

For the Landshoff process, it is merely necessary that each quark in one hadron comes within $1/Q$ of *one* of the quarks in the other hadron, Fig. 5.35(b), which is more probable. In order for this to match the same picture for the outgoing protons, the three intersections must line on a line transverse to the scattering plane, which gives a further suppression in the final result in Landshoff (1974).

5.10 Power-counting with multiple regions

The power-counting scheme of the preceding section arose from estimates of the sizes of propagator denominators around any given region R . We call this the canonical power

estimate. It not only gives us the power of Q associated with the region; it also indicates what kind of approximator is appropriate, where we neglect certain components of momentum on a line. Such approximators are critical to deriving factorization theorems.

So we must ask where the estimates fail. As we will now show, with a certain exception, the failures occur in two situations: (a) where the particular values of the intrinsic variables for R approach a smaller PSS; and (b) where the angular variables take us to the vicinity of a larger PSS. The true results in these cases are essentially obtained from the canonical power-counting for these other regions. The canonical power law of Q will be modified by logarithmic corrections. The one exception to the above statements concerns regions of the Glauber type, which are avoided by contour deformation in many cases, or otherwise need special discussion.

For high-order graphs there are many possible PSSs which intersect in many ways. An important feature of the following discussion will be to reduce the general case to a collection of a very few generic situations.

5.10.1 Locations of failures of power-counting

Consider a region R , with its radial variable λ . We use (5.29), (5.49) for the scaling of collinear and soft momenta, which gives the canonical sizes (5.73) for propagator denominators. Because of the normalization condition on the angular variables, the size of each momentum component is limited by its canonical scaling value, apart from a constant factor. Numerators are all bounded by their canonical values. Thus the only possibility of a failure of the power-counting is for one (or more) denominators to be much less than their canonical values.

To determine where this happens, we use a variation on the Libby-Sterman scaling argument. It involves the ratios of the propagator denominators to their canonical values:

$$r_l = \left| \frac{\text{denominator}_l}{\text{canonical}_l} \right|, \quad (5.89)$$

where l labels the line. Our concern is the minimum value of these ratios. First, suppose there is a non-zero lower bound to all the ratios: $r_l \geq r_{\min} \neq 0$, that applies uniformly over all propagators, over all the angular variables, over λ from zero to order Q , and for all large enough Q . Then the canonical value of the denominator is unambiguously correct for our power-counting.

Next we locate failures of such a bound by integrating around a surface of constant λ (Fig. 5.36) with the intrinsic coordinate(s) fixed. We call this surface $\Sigma(\lambda, R)$. Often the minimum value of the ratio is set by mass effects, so that the ratio is very small when λ is increased, thereby wrecking the power-counting. We therefore set masses to zero to give an appropriate diagnostic. If the minimum value of one or more ratios is zero in the massless theory, then the power-counting has failed, and we must examine a neighborhood of the subsurface where the minimum is zero. In this situation we have a singularity in the integrand in the massless theory.

Naturally, as in all our arguments, if it is possible to deform the contour of integration away from a singularity, we do so. Thus we only need treat cases where one or more of

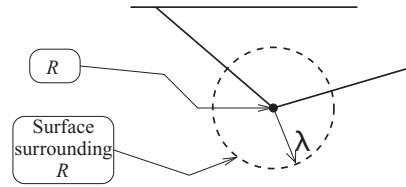


Fig. 5.36. The dashed line represents a surface $\Sigma(\lambda, R)$ of constant λ surrounding the PSS for R . The dot in the center represents the PSS R , and the three solid lines represent other PSSs. Although the surface $\Sigma(\lambda, R)$ is *diagrammed* as having radius λ , some momentum components may scale differently, e.g., as λ^2/Q .

the ratios r_l is pinched at zero. This is exactly the condition for a PSS, and in fact that the surface of constant λ intersects another PSS R' . There are now two cases, depending on whether or not the second PSS intersects the first.

If R' is like the upper solid line in Fig. 5.36, it does not intersect the original PSS R . In this case we reduce the maximum value of λ under consideration to avoid R' . The maximum value of λ is still of order Q , leaving our methodology unaltered. The region around R' can be treated by power-counting methods adapted to R' without the need to consider R . Any leftover gaps involve purely hard momenta.

The other case is that R' intersects the original PSS R , as for the lower two solid lines in Fig. 5.36. Then we must examine a neighborhood of R' , and use its power-counting to modify our original estimate – which we will do in Sec. 5.10.2. We can treat each such R' separately. In angular sectors not near these PSSs, the original estimate applies unchanged.

So one possible failure of the simple power-counting occurs at the intersection of $\Sigma(\lambda, R)$ with a PSS R' bigger than R .

But there are other possibilities for the intersection of the new surface R' with R . One is that the intersection $R' \cap R$ is a lower-dimension surface. In that case, we reorient the discussion. The intersection is itself a PSS, which we will call R_1 . Our power-counting applies for a fixed value of the intrinsic coordinates of R , in which case we treat R' and R as non-intersecting. We will separately treat the situation the intrinsic coordinates approach the position of a sub-PSS, of which R_1 will be a typical example.

A final possibility is that the intersection of R' with R has the same dimension as R , but is not the whole of R . There are possibly several such intersections. In that case we consider each of the intersections as a separate PSS. That is, we replace R by a set of PSSs which combine to form R . The edges of these small PSSs, particularly where they abut, are themselves lower-dimension PSSs.

It is also possible that the minimum value of one or more of the r_l ratios is non-zero on $\Sigma(\lambda, R)$ when λ is fixed, but that the minimum decreases to zero as $\lambda \rightarrow 0$. In other words the non-zero lower bound is not uniform in λ .⁸ This is behavior that we term Glauber-like, whose general criteria we will determine in Sec. 5.11.

⁸ We take for granted that if it is possible to deform the contour of integration to avoid such a situation, then we do so.

To see that the name is appropriate, we examine the quark and gluon propagators in Fig. 5.31(b). For a normal soft region, a soft denominator is of order λ^4/Q^2 , while a collinear denominator is of order λ^2 , for a large ratio

$$\frac{\text{collinear denom.}}{\text{soft denom.}} \sim \frac{Q^2}{\lambda^2}. \quad (5.90)$$

In our discussion of the Glauber pinch for Fig. 5.31(b), we used a soft transverse momentum of order m , which we now translate to $\lambda \sim \sqrt{mQ}$. In the Glauber region $k^\pm \sim m^2/Q$, so collinear denominators are of order m^2 , i.e., λ^4/Q^2 instead of λ^2 . Thus for a given gluon virtuality the collinear denominators are much smaller in the Glauber region than in the normal soft region.

The above discussion covers the case of fixed intrinsic coordinate(s) for the PSS R . A further issue occurs when we integrate over the intrinsic coordinate(s) of R , and approach a smaller PSS R_1 . This case is handled by observing that it involves the treatment of power-counting for the smaller region R_1 . If we change to the viewpoint of integrating around R_1 , we have treated that case already.

In summary, there are just two situations we need to cover: (a) the intersection of R with a bigger PSS R' at a generic point on R , which by a change of point-of-view also includes the approach on R to a smaller PSS; and (b) a Glauber-type situation.

5.10.2 Intersection of $\Sigma(\lambda, R)$ with PSS bigger than R

Relations between regions and subgraphs

Let R' be a PSS bigger than R , like one of the lower solid lines in Fig. 5.36, or the shaded surface in Fig. 5.32. We consider the integral over the constant λ surface $\Sigma(\lambda, R)$ near its intersection with R' , and we let λ' be the radial variable for R' .

Some of the propagators are not trapped at R' . Their denominators retain their powers from the first region, i.e., Q^2 for a hard line, λ^2 for a collinear line, and λ^4/Q^2 for a soft line. As we have already seen, the time scale for these lines is Q/λ^2 for the soft and collinear lines, or $1/Q$ for the hard lines; in all cases this is at most Q/λ^2 .

Since these lines are not pinched at R' , they constitute the hard subgraph H' for R' . When $\lambda \rightarrow 0$, the intersection of $\Sigma(\lambda, R)$ and R' approaches the original PSS R , which we can think of as an endpoint of R' . Thus in the situation we consider, i.e., $\lambda \ll Q$, the virtualities of some lines of H' are much smaller than the standard value Q^2 for a hard subgraph, the smallness being controlled by λ .

In contrast, the denominators of those lines that are pinched at R' have arbitrarily much smaller denominators, governed by λ' rather than λ . The time scale for these lines is Q/λ'^2 , much longer than that for the non-pinched lines. In the case of a graph for the Sudakov form factor, this is illustrated in Fig. 5.37. There, the placement of the collinear and soft subgraphs is meant to be like the space-time diagram Fig. 5.2(b).

With respect to each PSS, each line of the graph can be assigned a category: soft, collinear with respect to an external line, or hard. There are corresponding subgraphs: e.g., for the vertex graph we have subgraphs S, A, B, H with respect to R , and subgraphs S' ,

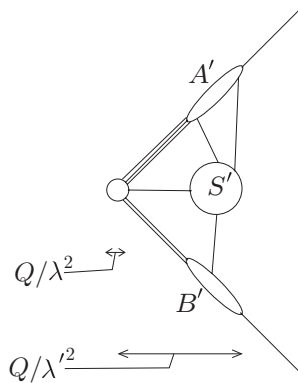


Fig. 5.37. Reduced graph for region R' near a smaller region R . The time scales for the different subgraphs are indicated.

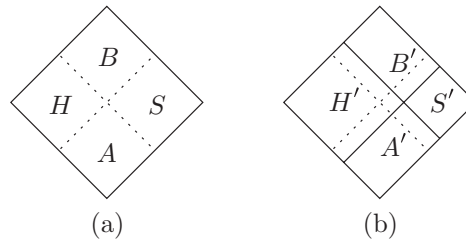


Fig. 5.38. Decomposition of graph into subgraphs for momentum classes, according to PSS (a) R and (b) $R' > R$. The subgraphs for R are delimited by the dotted lines and those for R' by solid lines.

A', B', H' with respect to R' . Now lines with energy of order Q on R retain approximately this energy near R' , while lines that are far off-shell at R are also far off-shell near R' . Thus we have the following possible transitions relating the categories of a line with respect to the different regions:

$$\begin{aligned}
 S &\rightarrow S', A', B', H'; \\
 A &\rightarrow A', H'; \\
 B &\rightarrow B', H'; \\
 H &\rightarrow H';
 \end{aligned}
 \tag{5.91}$$

as illustrated in Fig. 5.38.

As we integrate around $\Sigma(\lambda, R)$, λ' varies from zero to a maximum. We need to know the order of magnitude of the maximum value of λ' , which is in fact λ . To see this, we assign to the momentum components in S', A' and B' their canonical power-counting with respect to R' and match with the powers with respect to region R . The powers agree when $\lambda' \sim \lambda$. The only exception concerns the minus components for momenta in $S \cap B'$ and similarly for $S \cap A'$. These components would be of order Q for a fully collinear region,

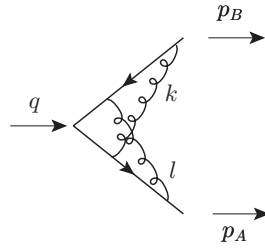


Fig. 5.39. Two-loop vertex graph.

but are now of order λ : the smallness of λ causes these momenta to be close to an endpoint of a collinear region by the standards of R' .

Example

A convenient illustration uses the two-loop graph in Fig. 5.39, with its two gluons of momenta k and l . Let region R be where k is soft and l is collinear to A . Thus the canonical sizes of (+, −, T) components are

$$R : \quad k \sim \left(\frac{\lambda^2}{Q}, \frac{\lambda^2}{Q}, \frac{\lambda^2}{Q} \right), \quad l \sim \left(Q, \frac{\lambda^2}{Q}, \lambda \right). \tag{5.92}$$

To avoid issues with IR problems, we assume the gluon is massive. Then the effective cutoff on λ is \sqrt{mQ} . We let the region R' be where k is collinear to B and l is hard:

$$R' : \quad k \sim \left(\frac{\lambda'^2}{Q}, Q, \lambda' \right), \quad l \sim (Q, Q, Q). \tag{5.93}$$

Now consider the particular orders of magnitude:

$$k \sim \left(\frac{m^{3/2}}{Q^{1/2}}, Q^{1/2}m^{1/2}, m \right), \quad l \sim (Q, Q^{1/2}m^{1/2}, Q^{3/4}m^{1/4}). \tag{5.94}$$

We could consider this as near to PSS R with $\lambda \sim Q^{3/4}m^{1/4}$: the components of l have exactly the standard sizes $(Q, \lambda^2/Q, \lambda)$ for a collinear-to- A momentum. All components of k are much less than Q , with a maximum size λ^2/Q , so k is soft. But notice that the plus and transverse components of k are much smaller than the standard λ^2/Q for a soft momentum.

But we can also consider the configuration as near to R' with $\lambda' \sim m^{3/4}Q^{1/4}$: we can treat k as collinear-to- B , since it has large negative rapidity: $y_k \sim -\frac{1}{2} \ln(Q/m)$, although l^- is much less than Q . We can consider l hard since its virtuality is much bigger than λ'^2 .

It can be checked that the time scales of the lines are

$$\begin{aligned} p_B - k - l &: \frac{1}{Q}, \\ l, p_A + k + l, p_A + l &: \frac{Q}{\lambda^2} \sim \frac{1}{Q^{1/2}m^{1/2}}, \\ k, p_B - k &: \frac{Q}{\lambda'^2} \sim \frac{Q^{1/2}}{m^{3/2}}. \end{aligned} \tag{5.95}$$

Thus we have a clear separation of scales, and the configuration has characteristics of both the regions R and R' . It can be verified that (5.94) gives a leading-power contribution. We must ensure that our treatment of factorization correctly handles it and the obvious myriad of similar possibilities in this and higher-order graphs.

In the above case, we assumed the gluon was massive, so the lower cutoff on transverse momentum was of order m , a typical mass. To keep k of low energy with respect to Q we were forced to keep its rapidity well short of that of p_B , and to put the lower quark lines far off-shell.

But if the gluon is massless, a rather more extreme situation arises. For example, try

$$k \sim \left(\frac{m^4}{Q^3}, \frac{m^2}{Q}, \frac{m^3}{Q^2} \right), \quad l \sim \left(Q, \frac{m^2}{Q}, m \right). \quad (5.96)$$

In the sense of rapidities, k is fully collinear to B : $y_k \sim -\ln(Q/m)$, and l is fully collinear to A : $y_l \sim \ln(Q/m)$. But k is also very soft by having its maximum component much less than Q . This configuration has $\lambda' \sim m^2/Q$, $\lambda \sim m$.

Obviously, we should not treat all such configurations separately, if at all possible, otherwise we could easily have much too complicated a problem to solve systematically. In fact we will be able to treat all such situations by a combination of methods that directly deal with the canonical scalings only.

But when we derive factorization, we will need to apply approximators suitable for neighborhoods of the different regions. Awareness of situations such as we have examined will inform our choice of approximators.

The physical property that will keep the situation under control is that the time scales associated with different lines are widely different, unlike the canonical case for the soft and collinear lines: we can treat one scale at a time and examine directly only the relations to neighboring time scales. Thus we only need to treat the relation between pairs of regions, each treated quite generically.

Effect on power-counting

To get the correct power-counting near the intersection of the constant λ surface $\Sigma(\lambda, R)$ and the PSS R' , we integrate over a range of λ of some particular order of magnitude, and then we decompose the result by the variable λ' , which measures the approach to R' . There will be powers of Q , λ and λ' :

$$Q^\alpha \lambda^\beta \lambda'^\gamma \quad (5.97)$$

appropriate to the strongly ordered situation $\lambda \ll \lambda' \ll Q$. To obtain the exponents we match to the canonical power-counting for the regions R and R' . The canonical power for region R' applies to the case that $\lambda \sim Q$ with $\lambda' \lesssim Q$. Thus we have

$$\text{power for } R' = Q^{\alpha+\beta} \lambda'^\gamma. \quad (5.98)$$

The canonical power for R applies when λ' has its maximum value, i.e., of order λ , so

$$\text{power for } R = Q^\alpha \lambda^{\beta+\gamma}. \quad (5.99)$$

This determines the powers in (5.97) from the canonical ones for R and R' .⁹

As in (5.75), the powers are those for the situation that we integrate over a range of a radial variable comparable to its size. Thus they are the sizes of integrands to be used in integrals with respect to $\ln \lambda$ and $\ln \lambda'$:

$$\int^{\ln Q} d \ln \lambda \int^{\ln \lambda} d \ln \lambda' Q^\alpha \lambda^\beta \lambda'^\gamma. \quad (5.100)$$

The lower limits of the integrals are either $\ln m$ or $\ln \sqrt{mQ}$, depending on whether the cutoff is governed by masses on collinear lines or masses on soft lines.

We now read off the results for the Q dependence of the integration over $\Sigma(\lambda, R)$.

The most common case we use is for the leading regions in QCD, for which $\beta = \gamma = 0$. Then the leading power of Q is Q^α , and the integrals over λ and λ' give logarithmic enhancements. Naturally we can have multiply nested regions. Iterating our argument gives the general rule that there is one logarithm of Q for each nesting. Thus for the one-loop Sudakov form factor, we have the nestings of leading regions: $H > A > S$, $H > B > S$. In (5.21), which depicts the hierarchy of regions, these nestings give ordered paths of length two and hence two logarithms. When we make the decomposition around the soft region, the two collinear regions A and B occur at distinct places in the angular integral. Thus the logarithms associated with the two different ordered paths add, rather than giving a more complicated situation.

In the other cases, one end or the other wins, which greatly simplifies the extraction of the leading power. There are several cases:

- If $\beta > 0$, then the top end $\lambda \sim Q$ of the λ integral wins. Then for the highest power of Q , the situation is the same as for region R' .
- If $\gamma > 0$, then the top end $\lambda' \sim \lambda$ of the λ' integral wins. Then for the highest power of Q , the situation is the same as for region R .

Note that if both $\beta > 0$ and $\gamma > 0$, the integral is dominated by $\lambda \sim \lambda' \sim Q$, i.e., by the hard region; both R and R' are non-leading by a power of Q .

- If both $\beta < 0$ and $\gamma < 0$, then the integral is dominated by the lower ends of both integrals. If they both have the same lower cutoff, then at the cutoff we have $\lambda' \sim \lambda$, which is just reproduces the generic situation for region R .

It is possible that the lower cutoffs are different: m for λ' and \sqrt{mQ} for λ . This needs special discussion.

- If $\beta < 0$ and $\gamma = 0$, then the lower end of the λ integral wins and there is at most a logarithm from the λ' integral. The power for R remains correct.

⁹ Situations where there is an apparent mismatch of power laws between regions were found in Bacchetta *et al.* (2008). These situations concern certain spin-dependent cross sections, and they can be handled by a generalization of our argument by allowing for powers of quark mass as well as of Q , λ , and λ' .

- If $\beta = 0$ and $\gamma < 0$, then the lower end of the λ' integral wins and there is a logarithm from the λ integral. The power for R' remains correct.

Aside from the case $\beta < 0$ and $\gamma < 0$, the general rule is that the overall power of Q is the highest power of Q as determined from the pure canonical powers for the individual regions.

5.11 Determination of Glauber-like regions

For each PSS, we found a canonical scaling law, and we saw that modifications to the canonical values of propagators were generally associated with canonical scaling for other intersecting PSSs. The only exception was what we called Glauber-like. This is where at some locations on the surface $\Sigma(\lambda, R)$ surrounding a PSS R , some denominators get much smaller than their canonical sizes, but that the ratio r_l on these lines only goes to zero at $\lambda = 0$.

We now show how to determine where the Glauber-like situation arises. We use another variation on the Libby-Sterman scaling argument, after first showing in an example how the Glauber region can be obtained from the standard scaling for a region by taking some of the angular coordinates to be very small.

5.11.1 Example

Consider Fig. 5.31(b) for the Drell-Yan process in the region where the quarks are collinear and the gluon is soft. With the canonical scalings, we parameterize the momenta of the gluon and the collinear momenta by

$$k = (S^+\lambda^2/Q, S^-\lambda^2/Q, S^T\lambda^2/Q), \quad (5.101a)$$

$$k_A = (z_A p_A^+, A^-\lambda^2/Q, A^T\lambda), \quad (5.101b)$$

$$k_B = (B^+\lambda^2/Q, z_B p_B^-, B^T\lambda). \quad (5.101c)$$

Here S^μ , A^μ , and B^μ give the angular coordinates for the soft and collinear momenta. Our usual normalization conditions show that the angular coordinates are at most about unity, and that the biggest is of order unity.

The canonical power-counting for this region applies when all the angular coordinates are of order unity. Note that in the interesting case that the transverse momentum of the Drell-Yan pair is of order m , a leading power is obtained only for $\lambda \sim m$, not for higher λ . When the gluon has a non-zero mass, the lowest effective value of λ is $O(\sqrt{mQ})$, and we get a power-suppression.

But we can also have a different scaling, the Glauber scaling, for which

$$k \sim (\lambda'^2/Q, \lambda'^2/Q, \lambda'), \quad (5.102a)$$

$$k_A \sim (Q, \lambda'^2/Q, \lambda'), \quad (5.102b)$$

$$k_B \sim (\lambda'^2/Q, Q, \lambda'), \quad (5.102c)$$

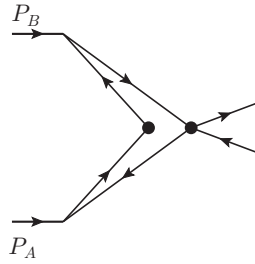


Fig. 5.40. Reduced diagram for Fig. 5.31(b) in Glauber region. The dots are the reduced vertices, and the lines are collinear to either p_A (in the bottom half of the diagram) or p_B (in the top half).

where we take all the coefficients of order unity. This can be obtained from the standard soft parameterization by making all the angular coefficients sufficiently small except for S^T :

$$S^\pm, A^-, B^+ \sim \lambda^2/Q^2, \quad A^T, B^T \sim \lambda/Q, \quad S^T \sim 1. \quad (5.103)$$

We follow this by the change of variable $\lambda' = \lambda^2/Q$.

From the point of view of the canonical soft scaling, this is a region where the soft denominator retains its canonical size, $\lambda^4/Q^2 = \lambda'^2$, but the collinear denominators are also of this size instead of their canonical value $\lambda^2 = \lambda'Q$. This is actually the minimum possible for the ratio of the collinear denominators to their canonical values, and approaches zero as $\lambda \rightarrow 0$.

We have seen that the integration contour is trapped in this region, unlike the case of DIS and e^+e^- annihilation

5.11.2 Application of Libby-Sterman argument

In the general case, with many loop momenta, there appears to be an explosion of the number of possible cases for different scalings of the momentum components, with a corresponding difficulty in determining the cases that are relevant. We overcome this problem by the Libby-Sterman method.

For some alternative scaling, we define a reduced diagram in which the vertices are obtained from those denominators with the canonical scaling. The lines of the reduced diagram are those with denominators that are much smaller than canonical. For the Glauber region of Fig. 5.31(b), the reduced diagram is obtained by shrinking the gluon to a point, to give Fig. 5.40.

We now apply the Landau criterion for a pinch in the massless version of the reduced diagram. This works just as in the standard Libby-Sterman argument. The only difference is in the interpretation of the vertices of the reduced graph: in the original argument, the vertices corresponded to subgraphs whose internal momenta are hard, with virtuality Q^2 . It is now possible to have vertices with much smaller internal virtualities. The common

feature is that the time and distance scales of the vertices of the reduced graph are much smaller than those for the lines.

The result is of the form of a possible PSS for the original graph. But the power-counting may have changed.

For a general starting region, some of the new PSSs are the same as leading PSSs of the original massless graph, so we can cover them by the original argument.

In Fig. 5.40 we have acquired a second hard scattering. The generic case would be to have multiple extra hard scatterings. These would be non-leading if all the hard scatterings had large virtuality. They are all covered by the original space-time diagram, Fig. 5.17(b), where the diagonal lines correspond to the on-shell lines in the reduced graph. What has changed with respect to the standard regions is that at the origin we have multiple colliding lines. Since each extra hard collision needs a minimum of two incoming and two outgoing on-shell lines, such a situation cannot arise in e^+e^- annihilation and DIS; in the hadronic part of these processes there is zero or one incoming hadron (respectively).

Viewing the space-time structure of the collision, Fig. 5.18, gives further intuition. Each incoming hadron contains multiple constituents which are located at a longitudinal distance $1/Q$ of each other, but with a transverse separation $1/M$. The single genuine hard collision has a quark out of one hadron getting within a transverse distance $1/Q$ of each other. The remaining constituents undergo soft collisions over a transverse range $1/M$; since these are soft collisions, the momentum transfer is restricted to small values, and the partons remain approximately collinear to their parent beams.

These situations are exactly of the kind that corresponds to spectator-spectator interactions with exchanged Glauber momentum. Therefore the Glauber region represents the general alternative scaling that we need to consider. The power-counting used for the Drell-Yan example readily generalizes to show that these situations contribute at leading power. Part of the factorization proof for the Drell-Yan process, in Ch. 14, will be to show a cancellation of the Glauber region.

Naturally, interesting variations on this theme can arise, e.g., if the transverse radius for the scattering differs substantially from the size of the hadron. This happens for nuclei. Similar adjustments to the picture are needed if the hard collision is at very large or small x , so that the size $1/Q$ of the hard collisions substantially differs from the longitudinal size of the fast-moving beam hadrons.

Exercises

5.1 (*)** From the coordinate-space representation of Feynman graphs (or otherwise), determine the regions in coordinate space that correspond to the regions R_H , R_A , R_B , R_S , $R_{A'}$, and $R_{B'}$ for the vertex graph. As far as possible determine the locations quantitatively.

There are some non-trivial complications in this problem because the final answer involves integrals over oscillating functions, with a lot of cancellation. A good answer probably involves significant original research.

If possible, verify the validity of estimates such as those given in Secs. 5.5.3 and 5.5.9, and that were used in the caption of Fig. 5.24.

- 5.2 (***)** The standard Landau-type analysis of singularities of Feynman graphs and of associated asymptotic problems is in momentum space. Reformulate it in coordinate space. The Coleman-Norton (Coleman and Norton, 1965) paper shows how the internal momentum configurations correspond to classical scattering processes. Show that this is literally true in a coordinate-space analysis.

Extend this result to treat asymptotics governed by nearby pinch singularities to show what regions of coordinate space dominate. Be as quantitative as possible. You should, for example, be able to recover the intuitive picture of the parton model, with its hard scattering on a short time scale on a constituent of a Lorentz-contracted, time-dilated hadron.

Are any corrections to this picture needed?

- 5.3 (***)** Find in the published literature, or construct for yourself, a proof that the Landau equations are actually necessary and sufficient for a PSS of a Feynman graph. To see that this is a non-trivial exercise, critically examine the accounts given in a standard textbook, e.g., Bogoliubov and Shirkov (1959); Eden *et al.* (1966); Itzykson and Zuber (1980); Peskin and Schroeder (1995); Sterman (1993). Are full proofs actually given? Do they actually work, and cover both necessity and sufficiency? Do they apply to the massless case, or do they make implicit assumptions only valid in the massive case?

You should also find or devise a proof that extends to certain modified integrals that occur in perturbative QCD. Such cases include graphs with eikonal propagators for Wilson lines: Ch. 10. These do not mesh particularly well with the Feynman-parameter representations often used in the treatments of the Landau equations.

For applications to pQCD, as we will see, it is important not merely to know that there is a PSS, but also to know exactly which lines participate in a particular pinch and which not, and to know exactly which loop-momentum variables actually participate in the pinch. Extend results in the literature to cover these issues explicitly.

Preferably any proof should be comprehensible by ordinary students of QFT.

- 5.4** Catalog the most general leading regions for graphs for the following processes. Describe the corresponding space-time structure.
- $q(P_A) + \gamma^*(q) \rightarrow q(p_B)$, i.e., the space-like version of the process treated in Sec. 5.3.1, with the state of momentum P_A in the initial state instead of the final state.
 - $H(P_A) + H(P_B) \rightarrow H(p_C) + X$, i.e., inclusive production of hadrons of large transverse momentum in hadron-hadron collisions.
- 5.5** For elastic hadron-hadron scattering, derive the power law given in Sec. 5.9.3 when there are multiple hard scatterings. Pay careful attention to the effects of momentum conservation at the hard scattering on the collinear loop integrals.

- 5.6** Extend the power-counting analysis given in Sec. 5.5 to the following cases:
- (a) other vertices replace the external electromagnetic current, e.g., a $\bar{\psi}\psi H$ vertex that might be for the interaction of a fermionic quark with a Higgs field;
 - (b) scalar quark in gauge theory.
- These represent possible variations on the basic ideas that might occur in applications of the Standard Model, or in extensions of it (e.g., scalar quarks appear in supersymmetric extensions).
- 5.7** Verify that the general rules given for power-counting apply in these specific cases. If not, improve the rules.
- 5.8** (***) Prove that the PSSs for a massless Feynman graph are flat surfaces.